ABCG transporters export cutin precursors for the formation of the plant cuticle

Elejalde-Palmett, Carolina; Martinez San Segundo, Ignacio; Garroum, Imène; Charrier, Laurence; De Bellis, Damien; Mucciolo, Antonio; Guerault, Aurore; Liu, Jie; Zeisler-Diehl, Viktoria; Aharoni, Asaph

Total number of authors:
15

Published in:
Current Biology

Link to article, DOI:
10.1016/j.cub.2021.02.056

Publication date:
2021

Document Version
Peer reviewed version

ABCG transporters export cutin precursors for the formation of the plant cuticle

Carolina Elejalde-Palmett[1], Ignacio Martinez San Segundo[2], Imène Garroum[1], Laurence Charrier[3], Damien De Bellis[1,4], Antonio Mucciolo[4], Aurore Guerault[1], Jie Liu[3], Viktoria Zeisler-Diehl[5], Asaph Aharoni[6], Lukas Schreiber[5], Bénédicte Bakan[7], Mads H. Clausen[2], Markus Geisler[3], Christiane Nawrath[1,*]

[1] Department of Plant Molecular Biology, University of Lausanne, CH-1015 Lausanne, Switzerland

[2] Center for Nanomedicine and Theranostics, Department of Chemistry, Technical University of Denmark, DK-2800 Kgs. Lyngby, Denmark

[3] Department of Biology, University of Fribourg, CH-1700 Fribourg, Switzerland

[4] Electron Microscopy Facility, University of Lausanne, CH-1015 Lausanne, Switzerland

[5] Institute of Cellular and Molecular Botany, University of Bonn, D-53115 Bonn, Germany

[6] Department of Plant Sciences, Weizmann Institute of Science, Rehovot 7610001, Israel

[7] INRAE, Biopolymers Interactions Assemblies UR1268, 44316 Nantes cedex 3, France

* Corresponding author and lead contact

Further information and requests for resources and reagents should be directed to and will be fulfilled by the Lead Contact, Christiane Nawrath (christiane.nawrath@unil.ch).

Summary

The plant cuticle is deposited on the surface of primary plant organs, such as leaves, fruits and floral organs forming a diffusion barrier and protecting the plant against various abiotic and biotic stresses. Cutin, the structural polyester of the plant cuticle, is synthesized in the apoplast. Plasma membrane-localized ABC-transporters of the G family have been hypothesized to export cutin precursors. Here we characterize *SlABCG42* of tomato representing an orthologue of *AtABCG32* in Arabidopsis. *SlABCG42* expression in Arabidopsis complements the cuticular deficiencies of the Arabidopsis *pec1/abcg32* mutant. RNAi-dependent downregulation of both tomato genes encoding proteins highly homologous to *AtABCG32* (*SlABCG36* and *SlABCG42*) leads to reduced cutin deposition and formation of a thinner cuticle in tomato fruits. By using a tobacco (*Nicotiana benthamiana*) protoplast system, we show that AtABCG32 and SlABCG42 have an export activity for 10,16-dihydroxy hexadecanoyl-2-glycerol, a cutin precursor *in vivo*. Interestingly, also free ω-hydroxy hexadecanoic acid as well as hexadecanedioic acid were exported furthering the research on the identification of cutin precursors *in vivo* and the respective mechanisms of their integration into the cutin polymer.

Keywords

ABC-transporter, acyl lipid, cutin, cuticle, wax, tomato, Arabidopsis, transport, plasma membrane, diffusion barrier

Introduction

A crucial step in the evolution of land plants has been the development of the cuticle, a particular surface structure of plant organs in primary growth stage that determines the surface properties of the organ [1]. The cuticle represents a diffusion barrier limiting transpirational water loss and other abiotic stresses and is playing an important role in plant defense by its impact on a wide variety of biotic interactions [1].

The main structural component of the cuticle is the polyester cutin that is composed of C16 and C18 fatty acids and their oxygenated derivatives, in particular hydroxy fatty acids, epoxy fatty acids and dicarboxylic acids, as well as glycerol and minor amounts of aromatic acids. 10, 16-dihydroxy hexadecanoic acid (10,16-diOH C16:0) is an aliphatic monomer present in the cutin of many species that may be very abundant, e.g. representing typically 70–80% in tomato fruit cutin and 60% of the Arabidopsis petal cutin [2-4]. Waxes composed of very long chain fatty acids and their derivatives as well as flavonoids and terpenoids impregnate the cutin polyester to form a functional cuticle. The structure of the cuticle and the composition of cutin and wax components vary according to species, organ, and developmental state [5].

A lot of progress has been made in the elucidation of cutin precursor formation. Briefly, fatty acids are synthesized in the plastid and are oxygenated at the ER. The transfer of acyl-CoA activated fatty acid derivatives to glycerol-3-phosphate by the glycerol-3-phosphate acyltransferases GPAT4, GPAT6, GPAT8 that have a phosphatase activity in addition to the acyltransferase activity result in mono acyl-2-glycerols [6-8]. In addition, numerous other precursors are generated by the action of acyltransferases of the BAHD family, including DEFICIENT IN CUTIN FERULATE (DCF) and DEFECTIVE IN CUTICULAR RIDGES (DCR) [9, 10].

The polymerization of cutin takes place in the apoplast within the cuticle and in the outermost layer of the cell wall. Several mechanisms of cutin polymerization and assembly have been investigated recently [5, 11]: Specific members of the GDSL-lipase family, such as CUS1 in tomato, are required for cutin synthesis acting via a trans-esterification mechanism [3, 12-15]. In addition, $\alpha\beta$ hydrolases, such as BODYGUARD, were proposed to structure the cuticle via a yet unknown mechanism, possibly polymerization [16, 17]. In addition, based on *in vitro* studies, a non-enzymatic

polymerization mechanism has been postulated that might be facilitated by pectin [18]. The finding that CUS1 of tomato can use 10, 16-diOH C16:0-*2*-glycerol as substrate to perform cutin oligomer/polymer synthesis by transesterification *in vitro* reinforced the model that mono hydroxyacyl-*2*-glycerols are cutin precursors *in vivo* [14].

For the export of cutin precursors, ATP-binding cassette (ABC) transporters of the G family have been proposed [19, 20]. Whereas half-size ABCGs seem to be ubiquitous, full-size or PDR-type ABCGs having a double nucleotide binding domain (NBD)-transmembrane domain (TMD) structure are restricted to plants and fungi [21, 22]. ABC transporters are capable of translocating molecules across cellular membranes against the electrochemical gradient using ATP as energy source. Despite being present in organisms of all kingdoms, plants have a highly enlarged number of the ABC-transporters of the C- and G-family in comparison to other eukaryotes, including mammals [23]. These are associated with the high number of metabolites that need to be transported within in the cell and have to be distributed within the plant organism or to its surfaces, serving as signals, such as plant hormones, being constituents of protective barriers or compounds toxic to biotic aggressors [24]. ABC-transporter diversity has been related to the developmental changes as well as adaptations to the aerial environment of terrestrial plants that keeping a sessile lifestyle acquired unique features to protect themselves against various abiotic and biotic stresses [19, 24].

Characterization of the *abcg11* mutant of Arabidopsis deficient in the AtABCG11 half-size transporter revealed its broad implication in the export of aliphatic molecules of the cuticle, including cutin monomers and aliphatic wax molecules [25-28]. While for the export of aliphatic wax molecules a dimerization with AtABCG12 is necessary, cutin precursors may be transported by the AtABCG11 homodimer, although heterodimerization with other AtABCG half transporters cannot be excluded [26]. The AtABCG13 half transporter is required for the formation of floral cutin in Arabidopsis [29]. Interestingly, while the ABCG11-type transporter is broadly present in all land plants and has often an increased number of homologues, AtABCG13 has been not identified in monocots and early diverging land plant lineages [30].

In addition, the full-size transporter ABCG32 of Arabidopsis has non-redundant functions in the formation of cutin in different organisms, particularly for cutins rich in

C16:0 monomers. The *pec1/atabcg32* mutant had reduced amounts of oxygenated cutin monomers (approximately 50%) in flowers and structural modifications of the interface of the cuticle with the cell wall in petals [31]. In Arabidopsis leaves that have a particular cutin rich in unsaturated C18 DCAs *AtABCG32* plays a more pronounced role in the early developing stages where the cutin has a higher proportion of C16 monomers [32]. In monocots having a mixed C16/C18 cutin composition, the knockout in the ABCG32-orthologue ABCG31 leads to an approximately 50% reduction in cutin and is associated with profound changes in cuticle thickness and ultrastructure [33, 34]. Considering the complexity of pathways involved in cutin formation a thorough investigation of the potential export functions of ABCG transporters for cuticular lipids is pertinent.

Here we show that SlABCG42 of tomato is a true orthologue of AtABCG32 since *SlABCGG42* expression under the control of the native *AtABCG32* promoter can complement the cutin deposition and the permeability of the cuticle in *pec1/atabcg32* flowers. Both AtABCG32 and SlABCG42 have very similar substrate specificities in the *Nicotiania benthamiana* protoplast assay exporting 10,16-diOH C16:0-*2*-glycerol, but also unesterified ω-hydroxylated C16:0 fatty acid as well as C16:0 dicarboxylic acid (DCA). AtABCG11, in contrast, does only transport 10,16-diOH C16:0-*2*-glycerol and the unesterifed ω–OH C16:0 acid, but not C16:0 DCA. Downregulation of *SlABCG42* together with the highly homologous gene*, SlABCG36,* in tomato leads to a decrease in fruit cuticle thickness and cutin amount, *i.e.* the amount of aliphatic monomers, in correlation to the expression level. Furthermore, cell size and surface structure were altered in the strongest downregulated line. These results show that ABCG32 transporters export various fatty acids and their derivatives, potentially supplying several pathways of cutin formation with precursors.

Results

SlABCG42 is a functional orthologue of AtABCG32

While in monocots and many dicot species, such as *Brassicae,* only a single gene with high homology to *AtABCG32* exists [30, 33, 34], tomato as well as other *Solanaceae* species own a second gene encoding a protein with high homology to AtABCG32 [35] (Figure S1A). Following the nomenclature by Ofori et al., *SlABCG36* (*Solyc05g018510*) encodes the closest AtABCG32 homologue, a protein of 75% identity and 85% similarity to AtABCG32 [35]. *SlABCG42* (*Solyc06g065670)* encodes for a protein of 69% identity and 79 % similarity to AtABCG32 and was thus called AtABCG32-like. This nomenclature differs from the one used by Lashbrooke et al. who named the *Solyc06g065670* gene product the ABCG32 homologue in tomato [36].

Although both, *SlABCG36* and *SlABCG42*, are expressed in the epidermis during tomato fruit development in accordance with a potential function cutin biosynthesis [37], *SlABCG36* has a much higher expression level than *SlABCG42* (Figure S1B) [37]. *SlABCG42* has nevertheless been reported to be regulated in its expression by the transcription factors MIXTA and ER4.1, similarly as other cutin biosynthesis genes [36, 38]. The question whether *SlABCG42* indeed represents a functional homologue of *AtABCG32* was addressed by expressing *SlABCG42* in the *pec1*/*atabcg32* mutant under the control of the AtABCG32 promoter.

Characterization of the floral cutin composition of several transgenic lines expressing *pAtABCG32::GFP-SlABCG42 in pec1/abcg32*, including *pec1*/*SlABCG42-L1* and *pec1*/*SlABCG42-L2* revealed complementation of the cutin deficiencies of the *pec1* mutant (Figure 1A, Figure S2) [31]. Although not all transgenic lines did complement the amount of floral cutin to 100% (Figure 1A), the expression of the GFP-tagged SlABCG42 transporter was able to complement the Arabidopsis cutin composition, *i.e.* not only cutin monomers present in tomato, such as 10,16-dihydroxy hexadecanoic acid (10,16-diOH C16:0), but also unusual cutin monomers typical for Arabidopsis cutin, *i.e.* 9,12-octadecadiendioic acid (C18:2 DCA) present in Arabidopsis flowers (Figure 1A, Figure S2).

Furthermore, the barrier properties of the petal cuticle were restored in both *pec1/SlABCG42* lines, as evaluated by TB staining (Figure 1B). The ultrastructure of

the petal cuticle in the *pec1/abcg32* mutant complemented with *pAtABCG32::GFP-SlABCG42* had the same structure as the one complemented with *pAtABCG32::GFP-AtABCG32* [31] (Figure 1C). The cuticular ridges were regular and filled by electron-dense cell wall material similar to Arabidopsis WT.

The complementation of the Arabidopsis *pec1/abcg32* mutant with *pAtABCG32::GFP-SlABCG42* demonstrates that the SlABCG42 transporter can exert AtABCG32 function in Arabidopsis that is hypothesized to be the export of cutin precursors [31].

AtABCG32 and SlABCG42 export mono-10,16-diOH C16:0-2-glycerol

In order to investigate whether AtABCG32 and SlABCG42 indeed have an export activity for cutin precursors, the *N. benthamiana* protoplast system was used that had been previously developed for the characterization of other ABC-transporters of Arabidopsis and tomato [39-41]**.** AtABCG32 fused to GFP at its N-terminus fully complemented *pec1/atabcg32* mutant phenotypes and was thus used for the activity study in *N. benthamina* [31] as well as an analogous construct generated for SlABCG42. In addition, constructs were generated to abolish transport activities by mutating the N-terminal Walker A motif required for ATP binding and hydrolysis, resulting in GFP-AtABCG32-M and GFP-SlABCG42-M, respectively (Figure S3A) [42]. Constructs for the expression of GFP-AtABCG32 and GFP-ABCG32-M as well as GFP-AtABCG32 and GFP-ABCG32-M under the control of the CaMV-35S promoter were Agrobacterium-transfected into *N. benthamiana* (Figure S3). Expression and localization at the plasma membrane (PM) of all the ABCG proteins epidermal cells of *N. benthamiana* were investigated by confocal laser microscopy. The expression of AtABCG32 and AtABCG32-M was in general stronger than of SlABCG42 and SlABCG42-M. Nevertheless, all ABCG transporters were at least partially localized at the PM based on the co-localization of the FP-tagged ABCGs with the PM-marker PIP2A-mCherry expressed under the CaMV-35S promoter as well as their localization adjacent the propidium iodine-stained cell wall (Figure S4) [43, 44]. FP-labeled proteins, PIP2A-mCherry as well as the FP-labelled ABCGs were often additionally localized to the endoplasmic reticulum, in particular when the expression level was high (Figure S4), probably due to saturation of the secretion system.

For studying the transport activity *N. benthamiana* cells transfected either with the functional or mutated GFP-AtABCG32 and GFP-SlABCG42 were loaded with [^{3}H[-10,16-diOH C16:0-2-glycerol, the most likely *in vivo* substrate, together with the unrelated substrate [^{14}C]-indole acetic acid ([^{14}C]-IAA). Both *N. benthamiana* cells expressing the functional GFP-AtABCG32 and GFP-SlABCG42 revealed significantly enhanced export of 10,16-diOH C16:0-2-glycerol in comparison with the vector control (Figure 2A and 2C, Figure S5). This was not the case for the auxin, IAA, an indolic substrate of ABCB-type ABC transporters (Figure 2B and 2D) [40], indicating substrate specificity for fatty acid compounds. Importantly, the Walker A mutated proteins revealed no export activity with 10,16-diOH C16:0-2-glycerol clearly indicating the ATP-dependency of this transport process and excluding indirect effects, like activation of secondary transport systems (Figure 2A and 2B). In summary, this dataset indicates that GFP-AtABCG32 and GFP-SlABCG42 catalyze the plasma membrane export of 10,16-diOH C16:0-2-glycerol in an ATP-dependent manner.

Previously, YFP-tagged AtABCG11 had been shown to complement the *atabcg11* mutant phenotypes (Bird et al., 2007). Therefore, YFP-AtABCG11 was expressed under the control of the CaMV-35S promoter in *N. benthamiana* cells (Figure S3A). Expression and localization at the PM of *N. benthamiana* cells was verified by confocal microscopy, as for the other ABCGs, see above (Figure S4). An export activity for [^{3}H]-10,16-diOH C16:0-2-glycerol, but not for [^{14}C]-IAA could be seen with YFP-AtABCG11, similar to these of AtABCG32 and SlABCG42 (Figure 2C and 2D; Figure S5).

Thus, all functional ABCGs transporters investigated here, *i.e.* AtABCG32, SlABCG42 and AtABCG11, transported specifically 10,16-diOH C16:0-2-glycerol in an ATP-dependent manner.

AtABCG32 and SlABCG42 transport also unesterified oxygenated fatty acids

In order to investigate further the specificity of AtABCG32 and SlABCG42 as well as AtABCG11, several commercially available ^{14}C-radiolabeled molecules that are also typical components of cutin, *i.e.* ω-OH C16:0 ([^{14}C]-ω-OH C16:0) and C16:0 DCA ([^{14}C]-C16:0 DCA) were tested in double labeling experiments with [^{3}H]-10,16-diOH C16:0-2-glycerol.

Interestingly, under our conditions the amount of [^{14}C]-ω-OH C16:0 molecules was reduced in the assay supernatant of the vector control in a time-dependent manner (Figure 2E; Figure S5). This apparent negative export (quantified by measuring radioactivity in the supernatant) represents a net import of unspecifically exported substrate, likely by yet uncharacterized import systems present in tobacco cells. However, again expression of GFP-AtABCG32, GFP-SlABCG42 and YFP-AtABCG11 significantly reduced this net import seen in the control, which can only be caused by an export activity for [^{14}C]-ω-OH-C16:0 (Figure 2E; Figure S5).

Similar as for [^{3}H]-10,16-diOH C16:0-2-glycerol, [^{14}C]-C16:0 DCA was released from the tobacco cells carrying the control construct and this release was enhanced by the presence of GFP-AtABCG32 and GFP-SlABCG42, but not by YFP-AtABCG11. These results indicate an export activity for C16:0 DCA of GFP-AtABCG32 and GFP-SlABCG42, but not of YFP-AtABCG11 (Figure 2F; Figure S5).

In summary, reduced import of [^{14}C]-ω-OH C16:0 and enhanced export of [^{14}C]-C16:0 DCA indicate an export activity of non-glycerol bound aliphatic C16:0 compounds for AtABCG32 and SlABCG42. An export of [^{14}C]-ω-OH C16:0, but not of [^{14}C]-C16:0 DCA demonstrates that ABCG11 has only a partially overlapping substrate specificity with AtABCG32 and SlABCG42 under the same assay conditions.

SlABCG36/42 mutants have reduced cutin deposition in the fruit cuticle

Tomato plants downregulated in the expression of *SlABCG36* and *SlABCG42* were generated by an RNAi approach. In the T2 generation *SlABCG42* expression was downregulated in expanding tomato fruits at 10 days after anthesis (DPA) by 95% in the strongest RNAi line expressing the *SlABCG42*-RNAi-fragment (Figure S6A). Interestingly, the expression of homologue *SlABCG36* was also reduced by 70%. Therefore, this RNAi-line was called *slabcg36/42-a*. In the T3 generation that was used for the complete characterization presented here the RNAi silencing was slightly less strong (90% for *SlABCG42* and 60% for *SlABCG36*). Downregulation of *SlABCG36* by the *SlABCG36*-RNAi fragment led to the reduction of *SlABCG36* expression by 60% in the strongest line of the T3 generation (10 DPA) (Figure 3A). As *SlABCG42* expression was also reduced in this line it was called *slabcg36/42-b*. Since the degree of downregulation of *SlABCG36* was similar between the RNAi-plants *slabcg36/42-a*

and *slabcg36/42-b*, differences in the phenotypes between both lines are likely due to the different reduction in *SlABCG42* expression, although changes in the level of RNAi-dependent downregulation of both SlABCG36 and AtABCG32 during fruit development may not be excluded [45].

Fruit cuticles of *slabcg36/42-a* and *slabcg36/42-b* were characterized at 20 DPA and in Red Ripe stage (~50 DPA). Although macroscopically the fruits did not show a difference to WT, the cuticle of both RNAi lines was strongly altered. While in WT not only the epidermis, but also subepidermal layers are cutinized, the cutinization of subepidermal layers is rather remnant in the RNAi lines at both developmental stages, as visualized by Sudan IV staining of cross-sections of the pericarp (Figure 3C). Furthermore, the cuticle thickness of the epidermis was reduced in the *slabcg36/42-b* and even more in the *slabcg36/42-a* at 20 DPA. Overall the cutinization was reduced by 35% in *slabcg36/42-b* and by 45% *slabcg36/42-a* at 20 DPA, when measuring the cutinized, *i.e.* Sudan VI-stained area. This reduction correlated well to the degree of the downregulation in the RNAi lines. The cutinization was also reduced in the RNAi lines at Red Ripe stage, even when less pronounced (19% and 24%, respectively).

Transmission Electron Microscopy (TEM) revealed alterations in the shape of the epidermal cells. In WT epidermal cells have a broad base and a conical top. At 20 DPA the epidermal cells were rounder in *slabcg36/42-b,* whereas in *slabcg36/42-a* the epidermal cells were much flatter and the conical top was barely visible (Figure 3C). These changes could also be well seen when the size of the ultrathin sections was quantified. The cells of WT and the intermediate downregulated RNAi-lines showed a high variability in size depending on where the section was taken. The *slabcg36/42-a* RNAi line having a rather flat shape showed less variability in section size that was overall smaller both at 20 DPA and in the Red Ripe stage (Figure 3C; Figure S6B), which corresponded well with the much smoother surface structure as visualized by Scanning Electron Microscopy (SEM) in both developmental stages (Figure 3C).

Alterations in cell shape which are likely a secondary effect of a reduced cutinization were much more pronounced in the stronger *slabcg36/42* line indicating that below a certain threshold potentially other regulatory mechanisms were activated. Altered surface morphology based on flatter epidermal cells had also been observed

in other strong cutin mutants, such as in *CUS1-, SlSHN3-* and *SlMIXTA-RNAi* lines [3, 36, 46].

The cuticular polyester of tomato fruits was characterized by GC-MS analysis at 20 DPA and the Red Ripe fruits stage. The principal cutin monomers were the C16 monomers 10,16-dihydroxy C16:0, ω-OH-C16:0, and C16:0 DCA. The only C18 monomer that could be detected was C18:0 DCA, which had very low abundancy (Figure 4A and 4B). Other monomers of low abundancy where not characterized in this study. The changes in the visible cutinization of the epidermal cell wall in *slabcg36/42-b* and *slabcg36/42-a* correlated to a reduction in the cutin amount (Figure 4A and 4B) as well as amount of the hydroxylated C16:0 acids, *i.e.* ω-OH C16:0 and 10, 16-diOH C16:0 that were reduced by approximately by 17% in *slabcg36/42-b* and 27% in *slabcg36/42-a* at 20 DPA as well as by 15% and 25% in Red Ripe tomato fruits, respectively (Figure 4A and 4B). 16:0 DCA and C18:0 DCA were not reduced in *slabcg36/42-b*, but reduced by approximately 50% in *slabcg6/42-a* in both developmental stages (Figures 4A and 4B). The lack in reduction of C16:0 DCA and C18:0 DCA was also observed in line *slabcg36/42-c,* another line carrying the construct for silencing *SlABCG36* that has an intermediate expression level for both genes (Figures S6A and S6C).

In summary, *slabcg36/42*-RNAi plants showed a reduction in all oxygenated cutin monomers investigated. The reason that C16:0 DCA and C18:0 DCA where only reduced in the strongest downregulated line might be due to differences in the affinity of the *SlABCG36* and *SlABCG42* transporters to different cutin precursors.

The reduction in 10, 16-diOH C16:0 was not accompanied by an alteration in the esterification level of its OH groups. The vast majority was esterified on both mid-chain and ω-OH position indicating that the reticulation pattern of the cutin polyester is not altered in *slabcg36/42*-RNAi plants in both stages of fruit development (Figure 4C). In this feature the cutin of *slabcg36/42*-RNAi plants was similar to this of the *gpat6* mutant of tomato that also does not have an alteration in the esterification pattern of 10, 16-diOH C16:0 [12].

Furthermore, the amount of ester-bound glycerol in the cutin was only reduced by approximately 15–20% in the stronger downregulated *slabcg36/42-a* line in both

stages of fruit development (Figure 4D) indicating only minimal changes in the structure of its fruit cutin.

Wax increase restores cuticle permeability in SlABCG36/42 compromised plants

The deposition of aliphatic wax components was assessed in *slabcg36/42*-RNAi plants revealing an increase of 20% and 30% at 20 DPA in *slabcg36/42-b* and *slabcg36/42-a*, respectively (Figure 5A). Particular, the odd-chain length alkanes (C29 and C31) were increased. In Red Ripe tomato fruits the variation in wax content was higher, not revealing a significant increase (Figure 5B). Thus, wax deposition was likely only indirectly affected by the downregulation of *SlABCG36* and *SlABCG42*.

Isolated, but not dewaxed cuticles of tomato fruits of *slabcg36/42*-RNAi lines did not exhibit an increased permeance to water, similar as seen in some other tomato fruit cuticle mutants [47] (Figure 5C). Only after the removal of wax from cuticles of tomato fruits at 20 DPA an increase in water permeance was identified. No differences were remarked in Red Ripe fruits in which the cuticle was over all less altered. The increased permeances of dewaxed cuticles at 20 DPA support the understanding that wax deposition plays a crucial role as barrier against transpirational water loss [48].

Discussion

ABCG transporters export cutin monomers

For the formation of the cuticular polyester cutin, the export of cutin precursors, from the epidermal cell to the apoplast, is essential. Genes encoding ABC-transporters of the G family are essential for cutin formation in many plant species, including monocots and dicots [25, 27, 28, 31, 34, 49]. Here we demonstrate that the ABCG half-size transporter AtABCG11 and the fully-size transporter AtABCG32, which are both required for cutin formation in Arabidopsis [25, 27, 28, 31] show export activity with ester-bound and free oxygenated fatty acids in a *N. benthamiana* protoplast system (Figure 2). In addition, SlABCG42, a homologue of AtABCG32 in tomato that is further characterized in these studies, exhibits similar export activity to AtABCG32.

The export activity for 10,16-diOH C16:0-2-glycerol of the investigated ABCG-transporters is well in accordance with our current understanding of cutin polymerization [7, 14, 50]. These results are also supported by the reduced 10,16-diOH C16:0 amounts in the cutin of the respective mutants as well as the restoration of the amounts of 10,16-diOH C16:0 in floral cutin by complementation of the *Arabidopsis pec1/abcg32* mutant with *AtABCG32* or *SlABCG42* or the *abcg11* mutant with *AtABCG11* [25, 27, 28, 31] as also shown in these studies (Figure 1 and Figure 4).

Interestingly, AtABCG32 and SlABCG42 exported not only 10,16-diOH C16:0 ester-bound to glycerol in the *N. benthamiana* protoplast system, but also the unesterified ω-OH C16:0 acid and C16:0 DCA suggesting that they recognize the aliphatic chain of the oxygenated fatty acid and not the configuration at the C1-carbon (Figure 2F). Whether AtABCG32 and SlABCG42 transport other types of acyl derivates than glycerol-bound derivatives during cutin synthesis needs future investigations.

The question whether AtABCG32 and SlABCG42 transport also molecules having a C18 backbone could not be directly addressed due to the lack of radiolabeled oxygenated C18 substrates commercially available. The complementation of C18:1 DCA and C18:2 DCA in the flower cutin of Arabidopsis by SlABCG42 and the reduction of the C18:0 DCA when *SlABCG36* and *SlABCG42* are strongly downregulated argue for a transport activity of molecules with a C18-backbone.

The export activity for 10,16-diOH C16:0-2-glycerol and free ω-OH C16:0 in *N. benthamiana* protoplasts expressing AtABCG11 (Figure 2E) supports in general the hypothesis that AtABCG11 exports cutin monomers as homodimer [26]. Interestingly, the substrate specificity of AtABCG11 differed from this of AtABCG32 and SlABCG42 since it did not export C16:0 DCA in the employed heterologous transport system arguing for an altered *in vivo* substrate specificity. However, at the moment we cannot rule out the theoretical but unlikely possibility that a functional heterodimerization with a tobacco half-size ABCG isoform or the lack of an Arabidopsis heterodimeric ABCG half forcing homodimerization has an influence on substrate specificities. Thus, ultimate proof of an altered substrate specificity for AtABCG11 awaits its *in vivo* confirmation.

While ABC-transporters are well characterized to transport a wide variety of metabolites, including many plant hormones, little is known about plant ABC-transporters transporting acyl lipids. Transport of acyl lipids from the endoplasmic reticulum to the chloroplast depends on the multicomponent ABC transport system with TGD1/AtABCGI14 being predicted to be the membrane permease of the ABC transporter that is localized to the inner plastidial membrane and is necessary to build the plastidial membrane system for photosynthesis [51]. The substrates of this transport system have not yet been identified, but are hypothesized to be phosphatidic acids [51]. The peroxisomal AtABCD1 that is required for β-oxidation exhibits transport activity for CoA-bound fatty acids, but not for free fatty acids [52]. Beyond cutin biosynthesis numerous ABCG half-size transporters are required for the formation of other polymers in the apoplast that are rich in lipids, such as suberin and sporopollenine [24]. Suberin is a polyester with a high amount of very-long chain fatty acids and fatty alcohols as well hydroxycinnamic acids. While the simultaneous knockout of AtABCG2, AtABCG6, AtABCG20 affects suberin synthesis in roots and seeds, the knockout of AtABCG1 and AtABCG16 affects pollen formation, potentially because of a function in sporopollenine formation [53]. The StABCG1 potato loss-of-function mutant that is most similar to AtABCG1 and ABCG16 of Arabidopsis affects, however, suberin formation in potato tubers [54]. Contribution of AtABCG1 to suberin formation in Arabidopsis could recently be shown [55]. The lack of information about the dimerization pattern of ABCG half transporters to functional transporters as well as the lack in knowledge about the structure of suberin precursors *in vivo* rendered the

characterization of the activity of suberin transporters difficult. Nevertheless, an enhanced ATP-hydrolyzing activity in the presence of very long chain fatty acids (C24-C30) and alcohols (C26-C30) of the purified AtABCG1 supported the hypothesis that this ABCG transporter exports suberin precursors in an unesterifed form [55]. Questions about the dimerization partners as well as identity of the substrates *in vivo* remain open, similarly as in our studies of AtABCG11 in cutin synthesis.

Plant ABCG-transporters may thus transport esterified and potentially also unesterified acyl-lipids across membranes.

AtABCG32 and SlABCG42 may transport particular derivatives of fatty acids

The cuticle of Arabidopsis petals is characterized by cuticular ridges having an amorphous cuticle proper and a more electron dense cuticular layer within the ridges [56]. In Arabidopsis, *AtABCG32* loss-of-function specifically affects the formation of regular cuticular ridges as well as the cuticle of young expanding leaves in the presence of functional AtABCG11 and AtABCG13 transporters [31]. The phenotypes of the *pec1/abcg32* mutant may be associated with the lack of particular cutin monomers exported by AtABCG32 that contribute to structuring the cuticle, as discussed in Bessire et al. and Fabre et al. [31, 32]. The tomato fruit has a thick reticulated cuticle that is also characterized by its content of cell wall components [57, 58]. The restoration of the ultrastructure of cuticular ridges in Arabidopsis by SlABCG42 points towards similar transport activities that are important for structuring the cuticle (Figure 1C).

In addition, *atabcg11* and *atabcg13* mutants have a strongly reduced cutin load and altered cuticle structure in leaves/stems and flowers, respectively, despite their functional AtABCG32 [25, 28, 29] which shows that ABCG-transporters do not function fully redundantly in cutin formation. Whether this partial lack in redundancy is related to a particular type of acyl lipid-derived cutin precursors that are transported by a specific transport system will remain open to future studies.

AtABCG32 orthologues of tomato are required for tomato fruit cutin formation

The modifications of the cuticle in *slabcg36/42*-RNAi plants comprise a reduced amount of cutin and a thinner cuticle at 20 DPA in correlation to the expression level

as well as a reduced amount of 10, 16-diOH C16:0 as well as ω-OH-C16:0 in the tomato fruit cutin (Figure 4A). Differences in the affinity of AtABCG32 and SlABCG36 and/or SlABCG42 might explain the lack in reduction of DCAs in the intermediate downregulated lines. Interestingly, AtABCG11 did not show a transport activity with C16:0 DCA in the protoplast system potentially pointing also to differences in affinity for this compound class among ABCGs required for cutin synthesis.

The molecular structure of the cutin of *slabcg36/42*-RNAi lines was unaltered similarly to the tomato *gpat6* mutant having also a reduced cutin amount, but no alterations in the esterification pattern of 10,16-diOH C16:0 (Figure 4C). This stands in contrast to the *cus1* mutant, where the esterification pattern of 10,16-diOH C16:0 was strongly altered [12]. The observed reduction in aliphatic cutin monomers in the *slabcg36/42*-RNAi lines and no other changes in cutin structure and composition support well the results of the SlABCG42 export activity for all oxygenated fatty acid derivatives.

The strongly down-regulated *slabcg36/42*-RNAi line exhibited in addition to the strongly reduced amount of cutin a particular strong cell flattening as well as a smaller cell size indicating broader effects on the properties of the cuticle and cell shape (Figure 3). Similar observations have also been made in other strong cutin mutants, including in *slmixta, slshine3*, *slcyp86a69* and *slgpat6* mutants of tomato [36, 46, 50]. The phenomenon might be related to alterations in regulatory pathways after sensing the lack in cell wall/cuticle integrity. There might, however, be some differences in the activated pathways among different cutin mutants. Indeed, unlike *slshine3 and slgpat6* mutants of tomato, no surface glossiness of the tomato fruits was observed in the *slabg36/42*-RNAi plants and the amount of glycerol was rather lower than higher in comparison to the *gpat6* mutant having a board range of changes in the gene expression of cutin biosynthesis genes [50, 59].

Tomato fruits of *slabcg36/42*-RNAi plants showed an increase in cuticular wax accumulation at 20 DPA likely compensating for the reduced cutin deposition since the permeability of the isolated cuticles was not significantly increased (Figure 5). Only dewaxed cuticles*, i.e*. cutin, of 20 DPA tomato fruits showed a significant increase in permeability highlighting the importance of wax for the impregnation of the cuticle [60]. An increase in aliphatic wax components has also been reported for *gpat6* and *cus1*

mutants of tomato [12, 59]. The increase in wax highlights that SlABCG36 and SlABCG42 are not required for wax export similarly as AtABCG32 [31].

Tomato fruits of *slabcg36/42*-RNAi plants in the Red Ripe stage exhibited still a significant reduction in the amount of cutin. However, the differences were weaker indicating that other transport systems likely contribute to cutin formation in later stages of tomato fruit development during which the gene expression of both *SlABCG36* and *SlABCG42* is low. In agreement with this also the cuticle of Red Ripe tomato fruits exhibited a better functionality, including better sealing properties to water and no increase in wax accumulation, similar as seen in mutants compromised in cutin biosynthesis in tomato fruits [47]. However, the surface of the strongest RNAi line remained flat indicating also persisting impact of the reduction in *SlABCG36* and *SlABCG42* expression on the cuticular morphology in Red Ripe tomato fruits (Figure 3C).

Since both *SlABCG36* and *SlABCG42* were downregulated in the RNAi downregulated plants little can be said about the exact contribution of SlABCG36 or SlABCG42 to the observed phenotypes. Remarkably, despite the more distant relation of SlABCG42 than SlABCG36 to AtABCG32, *SlABCG42* was consistently mentioned to be regulated together with other cutin biosynthetic genes, i.e. by MIXTA as well as by ER4.1 [36, 38]. A more detailed analysis of the specific roles of *SlABCG36* and *SlABCG42* in cutin biosynthesis will be the subject of future studies.

Transport of acyl lipid precursors by AtABCG transporters plays an essential role in cuticle formation

The current model of cutin synthesis could be greatly consolidated by our finding that the full-size ABCG-transporters AtABCG32 and AtABCG42 export 10,16-diOH C16:0-2-glycerol being cutin precursors *in vivo* [5]. That also the half-size ABCG-transporter AtABCG11 export acyl lipids represent an additional important piece of information despite the remaining uncertainties about the substrate specificity due to the impact of dimerization of the half transporters on the active site. Numerous questions that concern the elucidation of the export specificities *in planta* remain open, *i.e.* possible redundancies and specificities of the considerable number of other ABCG half transporters involved in cutin formation.

In the view of the broad specificity of the ABCG transporters associated with cutin synthesis for substrates containing an oxygenated acyl chain the questions remains open how the range of structures that represent cutin precursors *in* vivo is defined. Whether also unesterified monomers can be polymerized in the apoplast *in vivo* will need further investigations as well as the generation of potentially other more complex precursors containing an acyl chain within the epidermal cell. Up to now only the reaction mechanism of one enzyme polymerizing cutin in the apoplast has been characterized [14] that belongs to a large gene family encoding GDSL-type lipases/esterase proteins [61]. Furthermore, the reaction mechanism of members of the BODYGUARD clade, classified as αβ-hydrolases, which have been suggested to be required for cutin synthesis await characterization [16, 17].

Our findings support the model of a strongly diversified cutin biosynthesis pathway, including a high diversity of precursors, transport systems and polymerization mechanisms (Figure 6). Given the importance of cutin for the formation of a functional cuticle redundancies in the cutin biosynthetic pathway make sense, but also functional specializations can be expected.

Conclusions

The long-standing hypothesis that half-size and full-size ABCG transporters export the precursor 10, 16-diOH C16:0-2-glycerol for cutin formation [25, 31] has been experimentally confirmed by using a *N. benthamiana* protoplast system. Thus, direct transport of acyl lipids has been measured for the first time. The identification of unesterified hydroxy acids and dicarboxylic acids as potential substrate will require further research featuring the identity precursors and mechanisms of cutin polymerization and cuticle formation *in vivo*.

Acknowledgements

We thank Lacey Samuels (University of British Columbia) for providing us with the pEARLYGATE*_p35S::YFP-WBC11* plasmid. Margarita Plinar and Sagit Meir (Weizmann Institute) as well as Blaise Tissot (University of Lausanne) are thanked for their help with plant transformation and culture as well as Enrico Martinoia (University of Zürich) and Gauthier Mike L. Scavée (Technical University of Denmark) for helpful discussions. This work was supported by the Swiss National Science Foundation,

Switzerland (grants 31003A-125009, 31003A-146276 and 31003A-170127 to CN and 31003A-165877 to MG). M.H.C. is grateful to the Novo Nordisk Foundation (Denmark) for research support (grant no. 444-11319) and to DTU (Denmark) for a PhD scholarship to I.M.S.S.. L.S. was supported by the Deutsche Forschungsgemeinschaft, Germany.

Author contributions

Conceptualization, C.N., M.G.; Methodology, C.E.P., I.G., M.G.; Investigation, C.E.P, I.G., L.C., D.D.B., A.M., V.Z., B.B.; J.L.; Validation and Formal Analysis, C.E.P, I.G., M.G., LS; Resources, I.M.S.S., M.H.C., A.A.; Supervision, M.G., C.N.; Writing, C.N.; Funding acquisition, C.N.

Declaration of interests

The authors declare no competing interests.

Figure legends

Figure 1. *SlABCG42* complements *pec1/atacbg32* mutant phenotypes

(A) Transgenic *pec1* lines expressing *SlABCG42* (*pec1 SlABCG42-L1* and *L2*) under the native *PEC1* promoter complement the monomer composition (left) as well as cutin amount (right) in flowers of the *pec1* mutant. Statistically significant differences are indicated by different letters (Two-way ANOVA, Tukey HSD multiple comparison, $P<0.05$, n=5 replicates). DW, dry weight. The analysis was performed twice with similar results and a representative data set is shown. Selected monomers are presented here. See Figure S2 for complete data set. **(B)** The cuticle permeability is restored in the *pec1 SlABCG42-L1* and *L2* lines. Toluidine blue (TB) staining is shown in flowers of different genotypes. Scale bar = 1 mm. **(C)** The structure of cuticle in petals in the *pec1 SlABCG42-L2* line is similar to WT, as seen in *pec1* complemented with *AtABCG32* (*pec1 AtABCG32*) [22]. Transmission electron micrographs (TEM) of petals in different genotypes highlighting the cuticular proper (CP), cuticular layer (CL) and cell wall (CW) of the cuticular ridges of the petal cuticle. Black arrows indicate electron dense areas in the cuticular layer; white arrows indicate the lack of this electron dense area. Scale bars represent 1 µm. See also Figure S2.

Figure 2. ABCG transporters required for cutin formation export C16:0 derivatives

(A, B) In transport assays using *N. benthamiana* protoplasts, AtABCG32 and SlABCG42 show transport activity with 10,16-diOH C16:0-2-glycerol in contrast to transport-incompetent versions mutated in the Walker A domain (AtABCG32-M and SlABCG42-M). Percentage of initial export across the plasma membrane of protoplasts expressing the empty vector (Control), GFP-AtABCG32, GFP-AtABCG32-M, GFP-SlABCG42, and GFP-SlABCG42-M with different substrates measured after 20 min are shown: (A) [^{3}H]-labeled 10, 16-diOH 16:0-2-glycerol; (B) [^{14}C]-labeled indole acetic acid (IAA) used as unrelated compound for comparison. **(C-F)** Heterologous expression of AtABCG32 and SlABCG42 as well as AtABCG11 in *N. benthamiana* protoplasts reveals export activity across the plasma membrane for 10,16 diOH C16:0 as well as ω-OH C16:0, while C16:0 DCA is only exported by AtABCG32 and SlABCG42. Percentage of initial export after 20 min of different substrates across the plasma membrane of protoplasts expressing the empty vector (Control), YFP-AtABCG11, GFP-AtABCG32 and GFP-SlABCG42. Three radiolabeled C16:0 substituted acids were used as substrates: (C) 10, 16-diOH 16:0-2-glycerol; (E) ω-OH C16:0; (F) C16:0 dicarboxylic acid (C16:0 DCA). (D) Radiolabeled indole acetic acid (IAA) was used as unrelated compound for comparison. Data represented as mean ± standard error of the mean; multiple t-tests followed by Holm-Sidak multiple comparisons correction. Letters indicate significance groups; a = P<0.001 and b = P< 0.05; ns: not significant. See also Figure S3, Figure S4, and Figure S5.

Figure 3. Reduced expression of *AtABCG32*-homologous genes and fruit cuticle formation in *slabcg36/42*-RNAi plants

(A) Expression analysis of *SlABCG36* and *SlABCG42* in selected RNAi lines, i.e. *slabcg36/42-a* (*36/42-a*) and *slabcg36/42-b* (*36/42-b*) normalized to wild-type (WT) show significant differences between the RNAi lines in SlABCG42 expression as well as of both genes to WT. Real time-qPCR was performed with two biological replicates for 2 plants belonging to the same T3 line and three technical replicates by sample. Error bars represent SD. Analyses were performed with 10 DPA fruits. Statistically significant differences are indicated by different letters (Two-way ANOVA, Tukey HSD multiple comparison, P<0.05, n=4 replicates). The experiments were repeated twice

with similar results. **(B)** and **(C)** Reduced cutinization and altered epidermal cell shape were revealed in fruits of *slabc36/42* plants. (B) Reduction of the cutinization of the tomato fruit cuticle as visible by Sudan IV staining. Representative pictures (shown in C) were quantified by measuring the Sudan stained area in 5 pictures of 250 µm x 70 µm in size. Statistically significant differences between cuticle areas are indicated by different letters (One-way ANOVA, Tukey HSD multiple comparison, $P < 0.05$, $n = 15$ pictures). (C) Cross sections of the fruit exocarp are shown in light microscopy and transmission electron microscopy (TEM) as well as of the fruit surface in cryo-scanning-electron microscopy (SEM). Two developmental stages are shown: 20 DPA and Red Ripe. Sudan IV staining revealed cuticle and cutinized cells of the first exocarp cell layer. WT, wild type. Transmission electron microscopy (TEM) images showing cuticular layer and epidermal cells structure. EC: epidermal cell, CW: cell wall, CL: Cuticular layer. White bars = 10 µm. Black bars = 50 µm. See also Figure S1 and Figure S6.

Figure 4. Reduced cutin deposition in *slabcg36/42* fruits

The amount of the most abundant and selected minor cutin monomers (left) and the total cutin amount (right) present in isolated fruit cutins were quantified in 20 DPA-old **(A)** and in Red Ripe **(B)** fruits. Experiments were repeated at least twice and a representative set is shown here. Statistically significant differences between amount of cutin monomers and total cutin amounts are indicated by different letters (Two-way ANOVA, Tukey HSD multiple comparison, $P<0.05$, $n=4$ replicates). DW, dry weight. **(C)** Esterification levels of the different OH groups in 10,16-diOH C16:0 of cutin from fruits of wild-type (WT) and *slabcg36/42* lines are not different. Data were statistically analyzed by Two-way ANOVA, Tukey HSD multiple comparison, $P<0.05$, $n=5$ replicates. **(D)** Glycerol content in fruit cutin from the *slabcg36/42-a* plants is reduced. Statistically significant differences are indicated by different letters (Two-way ANOVA, Tukey HSD multiple comparison, $P<0.05$, $n=5$ replicates). See also Figure S6.

Figure 5. Wax deposition and water permeances of *slabcg36/42* fruit cuticles

Increased deposition of wax components (left) and total wax (right) of *slabcg36/42* tomato fruits in different stages **(A)** 20 DPA and **(B)** Red Ripe fruits. Statistically significant differences are indicated by different letters (Two-way ANOVA, Tukey HSD

multiple comparison, $P < 0.05$, $n = 5$ replicates). **(C)** Only dewaxed fruit cutins of *slabcg36/42* lines harvested at 20 DPA show increased permeability to water. The permeability of waxy and dewaxed cuticles was measured of 20 DPA and Red Ripe (RR) fruits. Student's *t*-test was used for assessing significant differences of wax components and water permeabilities when compared to WT (* = $p < 0.05$).

Figure 6. Schematic diagram of the function of ABCG-transporters in cutin formation

Full-size ABCG transporters, ABCG32 (AtABCG32 and its tomato orthologue SlABCG42), as well as half-size transporter AtABCG11 (G11) can export various types of cutin precursor classes across the plasma membrane. Individual substrate specificities for which evidence was presented in this study by transport assays in *N. bentahmiana* (bold) and by the analysis of loss/gain of function mutants are indicated below the transporters. Hypothesized precursors are marked by a question mark. Whether only esterifed or also unesterifed forms of oxygenated fatty acid are exported *in vivo* needs to be elucidated. Cutin precursors are exported to the apoplast where cutin is formed by different cutin synthases. The action of the ABCG transporters in cutin formation is highlighted in red. ABCG transporters that were characterized in this study are indicated in orange, other ABCG transporters that may be present, i.e. ABCG13 in petals, are indicated in grey. Blue ovals, CUTIN SYNTHASES of the GDSL-family; green ovals, BODYGUARD isoforms (having a hypothetical role in cutin polymerization); different shades of blue or green symbolize enzymes with potentially different enzymatic activities; cell wall material (CW) is depicted in brown, cutin in black and wax in grey; gradation indicates the complex composition of the cell wall/cuticle continuum.

STAR METHODS

RESOURCE AVAILABILITY

Lead contact

Further information and requests for resources and reagents should be directed to and will be fulfilled by the Lead contact Christiane Nawrath (christiane.nawrath@unil.ch).

Materials Availability

Plasmids generated in this study will be made available by the Lead contact. [^{3}H]-10,16-diOH C16:0 2-glycerol cannot be shared because of the regulations for shipment of radioactive material.

Data and Code Availability

Original data for the Figures in the paper will be made available upon request by the Lead contact.

EXPERIMENTAL MODEL AND SUBJECT DETAILS

Plant material

Arabidopsis thaliana accession Col-0, *Solanum lycopersicum* L. accession Micro-Tom and *Nicotiana benthamiana* were used in this work. The *Arabidopsis thaliana* mutant *pec1-2* was described previously [31]. All investigated genes are listed in Table S1. The primers for the identification of the T-DNA insertion are described in Table S2.

Growth conditions

A. thaliana plants were grown on soil in a Percival growth chamber under continuous light (100 mmol. m^{-2}. s^{-1}) at 20°C and 65% humidity for propagation, transformation, toluidine blue staining and floral cuticle analysis. *N. benthamiana* was grown on soil in a walk-in growth chamber at 63% humidity in a 16 h light/8 h dark cycle and 28 °C and 25°C, respectively. *S. lycopersicum cv* Micro Tom plants were grown on soil in the greenhouse, in which natural day light was supplemented with a sodium vapor bulb (250 µmoles/m^2/s) for 16 h (6 am to 10 pm), having a temperature of minimally 25°C for 12 h (6 am to 18 pm), 23°C for 3 h (6 pm to 9 pm) and 21°C for 9 h (9 pm to 6 am).

S. lycopersicum flowers were labelled at anthesis and fruits collected after 20-25 days for the 20 DPA stage and after 50 to 55 days for Red Ripe (RR) stage.

METHOD DETAILS

Chemical synthesis of tricium-labelled 2-mono (10,16-dihydroxyhexadecanoyl)glycerol ([^{3}H]-10,16-diOH C16:0 2-glycerol)

[^{3}H]-10,16-diOH C16:0 2-glycerol was synthesized from a custom-synthesized precursor that was supplied to Quotion Bioreserch, Cardiff.

A) Overview of the chemical synthesis of [^{3}H] 10,16-diOH C16:0 2-glycerol

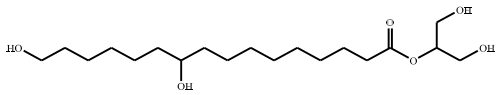

[^{3}H]-10,16-diOH C16:0 2-glycerol was synthesized in 7 steps from 1,10-decanediol **1** as shown in Scheme 1. **2** was prepared by protecting one of the hydroxyl groups of decane-1,10-diol with NAPBr. The other free alcohol was oxidized to the aldehyde by a Dess-Martin oxidation, to which was added the lithium acetylide 6-((tert-butyldimethylsilyl)oxy)hex-1-yne to afford the propargylic alcohol **3**. This alcohol was TBS protected to give triether **4**. The NAP group was removed with DDQ and H 2 O to give the primary alcohol **5**. The alcohol was subjected to a step-wise oxidation to the carboxylic acid, via successive Dess-Martin and Pinnick oxidations, which was then reacted with cis-5-hydroxy-2-phenyl-1,3-dioxane by Steglich esterification to form product **6**. Both TBS groups were removed with 20% aq. HF at 0 °C, to afford product **7**. The final product was afforded by reduction of 7 with tritium gas and Pearlman´s catalyst. Due to the requirements for dedicated facilities when working with tritium, tritium labelling was performed from precursor **7** by Quotient Bioresearch following a protocol developed in our laboratory for the deuteration of 7, but substituting deuterium by tritium. HRMS of the tritiated product showed a mixture of isotopically labelled products, in which the number of incorporated tritium atoms ranged from 0 to 4.

The radioactivity of **8** prevented its purification by recrystallization, so it was performed by HPLC. Non-isotopically labelled 10,16-diOH C16:0 2-glycerol was used to establish suitable HPLC conditions that prevented the migration of the ester from the secondary to a primary position of glycerol.

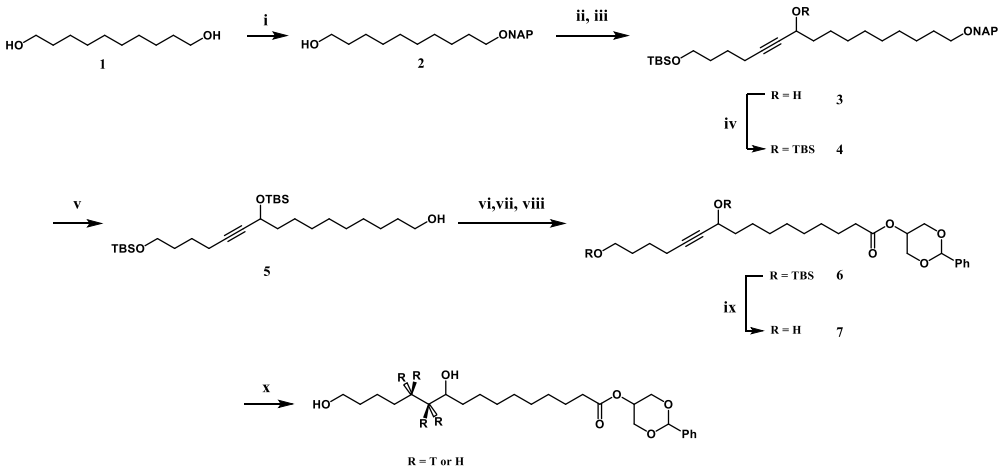

703

704 **Scheme 1**. Synthesis of [^{3}H]-10,16-diOH C16:0 2-glycerol. (***i***) NaH, 2-
705 (Bromomethyl)naphthalene, DMF/THF, 22 °C, 62 %; (***ii***) Dess-Martin periodinane,
706 CH_2Cl_2, 22 °C; (***iii***) 6-((*tert*- butyldimethylsilyl)oxy)hex-1-yne, *n*-BuLi, THF, -78 °C, 73
707 % (over two steps); (***iv***) TBSCl, imidazole, DMF, 22 °C, 76 %; (***v***) DDQ, H_2O, CH_2Cl_2,
708 22 °C, 64 %; (***vi***) Dess-Martin periodinane, CH_2Cl_2, 22 °C; **(*vii*)** $NaClO_2$, $NaHPO_4$
709 (aqueous, pH 3.5), 2-methyl-butene, *t*-BuOH, 22 °C; (***viii***) *cis*-hydroxy-2-phenyl-1,3-
710 dioxane, DMAP, EDC-HCl, 22 °C, 87 % (over three steps); (***ix***) 20 % aq. HF, MeCN, 0
711 °C, 69 %; (***x***) T_2, 20 % $Pd(OH)_2$/C, THF.

712 **B) Experimental procedures for the chemical synthesis of precursor 7**

713 10-(Naphthalene-2-ylmethoxy)decan-1-ol (**2**)

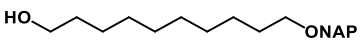

714 To a suspension of NaH (60% in oil, 3.44 g, 0.086 mol) in dry DMF (40 ml) at 0 °C
715 under an atmosphere of argon was added slowly a solution of 1,10-decanediol (15.00
716 g, 0.086 mol) in a mixture of THF and DMF (30 and 40 ml respectively). The resulting
717 mixture was let to warm slowly to 20 °C. After 2 h, a solution of NAPBr (9.52 g, 0.043
718 mol) in dry DMF (30 ml) was added dropwise. The reaction was stirred for 16 h and
719 excess reagent was quenched by addition of ice until bubbling ceased. The mixture
720 was extracted with Et_2O (3 × 200 ml). The combined organic phases were washed with
721 sat. aq. NaCl (200 ml), dried with $MgSO_4$, filtered, concentrated and purified by flash
722 chromatography (EtOAc/heptane 1:4) affording **2** as a white solid (8.44 g, 62%). **R_f**
723 (EtOAc/heptane 1:4) = 0.16; **mp**: 60–62 °C; **^{1}H NMR** (400 MHz, $CDCl_3$) δ 7.86–7.80
724 (m, 3H), 7.78 (s, 1H), 7.51–7.43 (m, 3H), 4.67 (s, 2H), 3.63 (t, *J* = 6.6 Hz, 2H), 3.51 (t,
725 *J* = 6.7 Hz, 2H), 1.69–1.60 (m, 2H), 1.60–1.51 (m, 2H), 1.44–1.23 (m, 12H); **^{13}C NMR**
726 (101 MHz, $CDCl_3$) δ 136.4, 133.4, 133.1, 128.2, 128.0, 127.8, 126.4, 126.2, 125.9,

125.9, 73.1, 70.7, 63.2, 32.9, 29.9, 29.7, 29.7, 29.6, 29.5, 26.3, 25.9; **HRMS (MALDI+)** $C_{21}H_{30}O_2$, m/z [M+Na^+] 337.2138, found 337.2140.

1-((*tert*-Butyldimethylsilyl)oxy)-16-(napththalene-2-ylmethoxy)hexadec-5-yn-7-ol (**3**)

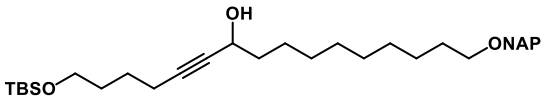

To a mixture of DMP (6.63 g, 15.63 mmol) in CH_2Cl_2 (25 ml) was added slowly a solution of **2** (3.78 g, 12.02 mmol) in CH_2Cl_2 (20 ml). The resulting mixture was stirred for 1.5 h and poured into an aqueous solution of $Na_2S_2O_3$ (35 g in 200 ml). The mixture was stirred vigorously for 5 min and extracted with Et_2O (200 ml). The organic phase was washed with sat. aq. $NaHCO_3$ (200 ml), dried with $MgSO_4$ and concentrated, and used in the subsequent reaction without further purification.

To a solution of **2** (3.32 g, 15.64 mmol) in THF (15 ml) at -78 °C under an atmosphere of nitrogen was added dropwise *n*-BuLi (6.7 ml, 2.7 M in pentane, 18.05 mmol). The resulting mixture was allowed to warm slowly to 20 °C and a solution of the crude aldehyde (3.760 g, 12.0 mmol) in dry THF (15 ml) was added. The resulting mixture was stirred for 16 h, poured into sat. aq. NH_4Cl (100 ml) and extracted with CH_2Cl_2 (3 × 100 ml). The combined organic phases were dried with $MgSO_4$, filtered, concentrated and purified by flash chromatography (EtOAc/heptane 1:9) affording **3** as a yellow oil (4.12 g, 65%); $\mathbf{R_f}$ (EtOAc/heptane 1:9) = 0.17; **^{1}H NMR** (400 MHz, $CDCl_3$) δ 7.86–7.80 (m, 3H), 7.78 (s, 1H), 7.51–7.45 (m, 3H), 4.67 (s, 2H), 4.34 (tt, *J* = 8.9, 4.1 Hz, 1H), 3.62 (t, *J* = 6.0 Hz, 2H), 3.51 (t, *J* = 6.7 Hz, 2H), 2.23 (td, *J* = 6.7, 1.7 Hz, 2H), 1.72–1.53 (m, 8H), 1.48–1.25 (m, 12H), 0.91 (s, 9H), 0.05 (s, 6H); **^{13}C NMR** (101 MHz, $CDCl_3$) δ 136.36, 133.44, 133.08, 128.24, 127.99, 127.82, 126.40, 126.16, 125.91, 125.88, 85.41, 81.69, 73.09, 70.67, 62.90, 62.79, 38.35, 32.06, 29.94, 29.66, 29.64, 29.61, 29.42, 26.35, 26.10 (3C), 25.36, 25.27, 18.64, 18.48, -5.14 (2C); **HRMS (MALDI+)** $C_{33}H_{52}O_3Si$, m/z [M+H+] 525.3578, found 525.3593.

1,7-Bis((*tert*-Butyldimethylsilyl)oxy)-16-(naphthalen-2-ylmethoxy)hexadec-5-yne (**4**)

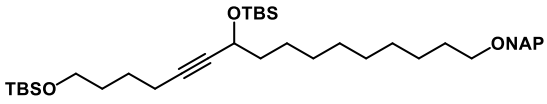

To a solution of **4** (4.12 g, 7.86 mmol) in dry DMF (20 ml) under an atmosphere of nitrogen was added imidazole (0.803 g, 11.80 mmol) and TBSCl (1.54 g, 10.22 mmol). The reaction mixture was stirred for 18 h, poured into sat. aq. NH_4Cl (100 ml) and was extracted with CH_2Cl_2 (3 × 100 ml). The combined organic phases were dried with $MgSO_4$, filtered, concentrated and purified

by flash chromatography (EtOAc/heptane 1:19) affording **4** as a colourless oil (3.54 g, 71%); $\mathbf{R_f}$ (EtOAc/heptane 1:19) = 0.33; **^{1}H NMR (400 MHz, $CDCl_3$)** δ 7.85–7.80 (m, 3H), 7.78 (s, 1H), 7.50–7.43 (m, 3H), 4.67 (s, 2H), 4.31 (tt, *J* = 6.6, 1.9 Hz, 1H), 3.61 (t, *J* = 6.0 Hz, 2H), 3.51 (t, *J* = 6.6 Hz, 2H), 2.21 (td, *J* = 6.9, 1.9 Hz, 2H), 1.68–1.50 (m, 8H), 1.37 (m, 4H), 1.28 (d, *J* = 2.9 Hz, 8H), 0.90 (s, 9H), 0.89 (s, 9H), 0.12 (s, 2H), 0.10 (s, 3H), 0.04 (s, 6H); **^{13}C NMR (101 MHz, $CDCl_3$)** δ 136.36, 133.44, 133.08, 128.22, 127.98, 127.81, 126.38, 126.14, 125.89, 125.86, 84.27, 82.37, 73.08, 70.67, 63.36, 62.78, 39.17, 32.09, 29.95, 29.69, 29.67, 29.62, 29.42, 26.36, 26.10 (3C), 26.01 (3C), 25.49, 25.31, 18.65, 18.46, 18.43, -4.28, -4.81, -5.16 (2C); **HRMS (MALDI+)** $C_{39}H_{66}O_3Si_2$, m/z [M+Na$^+$] 661.4443, found 661.4445.

10,16-Bis((*tert*-butyldimethylsilyl)oxy)hexadec-11-yn-1-ol (**5**)

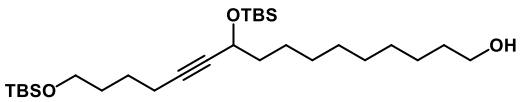

To a solution of **4** (3.47 g, 5.431 mmol) in CH_2Cl_2 (85 ml) was added DDQ (1.85 g, 8.15 mmol) and H_2O (20 ml). After 16 h, the mixture was poured into sat. aq. $NaHCO_3$ (100 ml), and was extracted with CH_2Cl_2 (3 × 100 ml). The combined organic phases were dried with MgSO4, filtered, concentrated and purified by flash chromatography (EtOAc/heptane 1:9) affording **5** as a colourless oil (1.95 g, 72%); $\mathbf{R_f}$ (EtOAc/heptane 1:4) = 0.29; **^{1}H NMR** (400 MHz, $CDCl_3$) δ 4.31 (tt, *J* = 6.6, 2.0 Hz, 1H), 3.66–3.58 (m, 4H), 2.21 (td, *J* = 6.9, 2.0 Hz, 2H), 1.67–1.50 (m, 8H), 1.45–1.24 (m, 12H), 0.90 (s, 8H), 0.89 (s, 9H), 0.11 (s, 3H), 0.09 (s, 3H), 0.04 (s, 6H); **^{13}C NMR** (101 MHz, $CDCl_3$) δ 84.30, 82.36, 63.36, 63.23, 62.81, 39.17, 32.96, 32.11, 29.68, 29.64, 29.56, 29.41, 26.11 (3C), 26.02 (3C), 25.88, 25.48, 25.32, 18.67, 18.48, 18.45, -4.28, -4.81, -5.15 (2C); **HRMS (MALDI+)** $C_{28}H_{58}O_3Si_2$, *m/z* [M+Na$^+$] 521.3817, found 521.3825.

cis-2-Phenyl-1,3-dioxan-5-yl 10,16-bis((*tert*-butyldimethylsilyl)oxy)hexadec-11-ynoate (**6**)

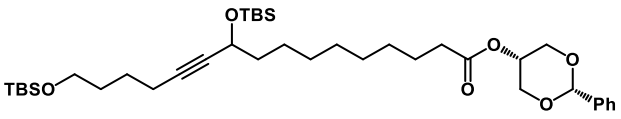

To a mixture of DMP (1.25 g, 2.95 mmol) in CH_2Cl_2 (30 ml) was added slowly a solution of **5** (1.13 g, 2.27 mmol) in CH_2Cl_2 (30 ml). The resulting mixture was stirred for 2.5 h and poured into a solution of $Na_2S_2O_3$ (45 g) in sat. aq. $NaHCO_3$ (250 ml). The mixture was stirred vigorously for 5 min and then extracted with Et_2O (200 ml). The organic phase was washed with sat. aq. $NaHCO_3$ (200 ml), dried with $MgSO_4$, concentrated and used in the subsequent reaction without further purification.

To a solution of the crude aldehyde (1.24 g) in *t*-BuOH (100 ml) was added 2-methyl-2-butene (3.180 g, 4.8 ml, 45.34 mmol) and an aqueous solution (27 ml) of NaH_2PO_4 (2.18 g, 18.14 mmol) and $NaClO_2$ (0.267 g, 2.95 mmol). After 15 h, a buffer aqueous solution of NaH_2PO_4 was added (0.66 M, 100 ml) and the mixture was extracted with CH_2Cl_2 (3 × 150 ml). The combined organic phases were washed with sat. aq. NaCl (200 ml), dried with Na_2SO_4, filtered, concentrated, and used in the subsequent reaction without further purification.

To a solution of the crude carboxylic acid (1.47 g) in dry CH_2Cl_2 (100 ml) under an atmosphere of nitrogen was added *cis*-5-hydroxy-2-phenyl-1,3-dioxane (0.531 g, 2.946 mmol), DMAP (0.472 g, 3.852 mmol) and EDCI (0.660 g, 3.399 mmol). After 15 h, the reaction mixture was concentrated, taken on silica and purified by flash chromatography (EtOAc/hetane 1:9), affording **17** as a transparent oil (0.609 g, 40%); $\mathbf{R_f}$ (EtOAc/heptane 1:9) = 0.22; **^{1}H NMR** (400 MHz, $CDCl_3$) δ 7.55–7.47 (m, 2H), 7.41–7.32 (m, 3H), 5.56 (s, 1H), 4.74–4.69 (m, 1H), 4.34–4.13 (m, 5H), 3.61 (t, *J* = 6.1 Hz, 2H), 2.43 (t, *J* = 7.6 Hz, 2H), 2.21 (td, *J* = 6.8, 1.8 Hz, 2H), 1.73–1.50 (m, 8H), 1.47–1.21 (m, 10H), 0.90 (s, 9H), 0.89 (s, 9H), 0.11 (s, 3H), 0.10 (s, 3H), 0.06–0.03 (m, 6H); **^{13}C NMR** (101 MHz, $CDCl_3$) δ 173.99, 137.97, 129.19, 128.41 (2C), 126.16 (2C), 101.35, 84.27, 82.33, 69.26 (2C), 65.83, 63.33, 62.78, 39.14, 34.52, 32.08, 29.53, 29.37 (2C), 29.24, 26.08 (3C), 26.00 (3C), 25.47, 25.29, 25.06, 18.64, 18.45, 18.42, -4.30, -4.82, -5.17 (2C); **HRMS (MALDI+)** $C_{38}H_{66}O_6Si_2$, m/z [M+Na$^+$] 697.4290, found 697.4243.

cis-2-Phenyl-1,3-dioxan-5-yl 10,16-dihydroxyhexadec-11-ynoate (**7**)

To a solution of **6** (0.975 g, 1.445 mmol) in MeCN (145 ml) at 0 °C was added 20% aq. HF (6 ml, 69 mmol). The resulting

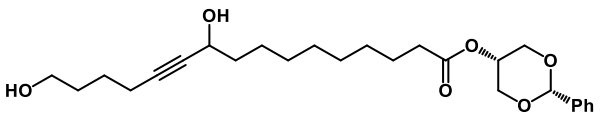

mixture was stirred at 0 °C for 4 h. TMSOEt (33 ml) was added, and the mixture was stirred for 30 minutes, poured into sat. aq. NH_4Cl (200 ml) and extracted with CH_2Cl_2 (3 × 200 ml). The combined organic phases were dried with $MgSO_4$, filtered, concentrated and purified by flash chromatography (EtOAc/hetane 6:4), affording **7** as a white solid (0.354 g, 55%); $\mathbf{R_f}$ (EtOAc/heptane 6:4) = 0.16; **mp**: 50–52 °C; **^{1}H NMR** (400 MHz, $CDCl_3$) δ 7.58–7.46 (m, 2H), 7.45–7.31 (m, 3H), 5.56 (s, 1H), 4.72 (s, 1H), 4.38–4.25 (m, 3H), 4.17 (d, *J* = 13.2, 2H), 3.65 (t, *J* = 6.3 Hz, 2H), 2.43 (t, *J* = 7.5 Hz, 2H), 2.25 (td, *J* = 6.8, 2.0 Hz, 2H), 1.74–1.54 (m, 10H), 1.50–1.24 (m, 10H); **^{13}C NMR**

(101 MHz, $CDCl_3$) δ 174.04, 137.94, 129.23, 128.44 (2C), 126.17 (2C), 101.38, 85.16, 81.89, 69.28 (2C), 65.87, 62.84, 62.47, 38.27, 34.52, 31.91, 29.43, 29.29, 29.24, 29.19, 25.26, 25.06, 25.05, 18.62; **HRMS (MALDI+)** $C_{26}H_{38}O_6$, m/z [M+Na^+] 469.2561, found 469.2563.

1,3-Dihydroxypropan-2-yl 10,16-dihydroxyhexadecanoate-11,11,12,12-t_4 (**8**)

The final product **8** (for chemical structure: see Scheme 1) was synthesized by Quotient Bioresearch by adapting a protocol developed in our laboratory for the deuteration of **7**, shown below. This was done by substituting deuterium by tritium, as well as modifying the method of purification. The radioactivity of **8** prevented its purification by recrystallization, so it was instead purified by HPLC (Column: Zorbax Eclipse XDB-C8 5 µm 150 x 4.6 mm. Elution was carried out combining eluent A (5 mM NH_4Ac in H_2O) and eluent B (5 mM NH_4Ac in 90% aq. MeCN) in the following fashion: 20% B for 1 minute, gradual increment of B to 30% for 4 minutes, gradual increment of B to 40% for 15 minutes, then sudden reduction of B to 20% and hold for 3 minutes. Total run time: 23 min). **TOF MS ES$^-$** $C_{19}H_{34}T_4O_6$, m/z [M+FA-H^+] 415.2971, found 415.2947. **Radiochemical purity (RCP)**: 91.6 % **Specific activity**: 86 Ci/mmol

C) Procedure for the deuteration of 7 supplied to Quotient Bioresearch

1,3-Dihydroxypropan-2-yl 10,16-dihydroxyhexadecanoate-11,11,12,12-d_4

To a solution of **7** (0.169 g, 0.378 mmol) in dry THF (20 ml) under an atmosphere of nitrogen was added 20% $Pd(OH)_2/C$ (40 mg). A deuterium atmosphere was installed by bubbling D_2 through the solution for 5 minutes. The reaction mixture was stirred under a D_2 atmosphere for 15 h filtered through Celite, concentrated and recrystallized from EtOAc and heptane, affording **9** as a white solid (96 mg, 69%); **mp**: 56–58 °C; **^{1}H NMR** (400 MHz, MeOD) δ 4.94–4.88 (m, 1H), 3.70 (dd, *J* = 12.4, 5.3 Hz, 2H), 3.65 (dd, *J* = 12.0, 6.0 Hz, 2H), 3.55 (t, *J* = 6.6 Hz, 2H), 3.52–3.48 (m, 1H), 2.38 (t, *J* = 7.4 Hz, 2H), 1.68–1.59 (m, 2H), 1.58–1.49 (m, 2H), 1.48–1.24 (m, 16H); **^{13}C NMR** (101 MHz, MeOD) δ 175.34, 76.53, 62.99, 61.70 (2C), 38.38, 35.15, 33.64, 30.79, 30.59, 30.37, 30.17, 26.78, 25.98; **HRMS (MALDI+)** $C_{19}H_{34}D_4O_6$, m/z [M+Na^+] 389.2812, found 389.2827.

Isolation of *N. benthamiana* protoplasts

Protoplasts were prepared as previously described by Geisler et al., 2005 [62]. Shortly, Agrobacterium-infiltrated leaves of four-weeks-old *N. benthamiana* plants were

857 abraded with abrasive paper P500 and the abaxial part was put in contact with ½ MCP
858 medium (500 mM D-Sorbitol, 10 mM 2-(N-morpholino) ethanesulfonic acid (MES), 1
859 mM $CaCl_2$, pH 5.6). Incubated leaves in digestion buffer (MCP with 1% cellulose YC,
860 1% pectolyase Y23, 1% bovine serum albumin (BSA)) for 90 min at 30°C. Solution was
861 filtered through a 320-mesh stainless steel filter and protoplasts were purified using
862 MCP medium with 100% Percoll pH 6 cushion at the bottom of the tube. Tubes were
863 centrifugated for 10 min at 4°C at 1500 rpm, no brake. Protoplasts resuspended in up
864 to 5 mL of 100% Percoll pH 6. A gradient was built from bottom to top by overlaying
865 carefully: protoplasts in 100% Percoll pH 6, 1 Vol. Percoll 25% (in CP), and 5 mL MCP
866 and centrifuged at 1200 rpm, 10 min, 4°C, no brake. Protoplasts were recovered from
867 the Percoll 25%/MCP interphase.

868 **Generation of constructs**

869 All primers that are mentioned in the following description of the cloning strategies are
870 listed in Table S2. Constructs for the expression of SlABCG42 in *A. thaliana*: Genomic
871 DNA from *S. lycopersicum cv* Micro Tom was isolated by 500 mg of grinded young
872 leaves, extraction with CTAB buffer (1.4 M NaCl, 100 mM Tris– HCl pH 8, 20 mM EDTA
873 pH 7.8, 2% CTAB and 0.2% 2-mercaptoethanol) and a subsequent purification using
874 phenol/chloroform/isoamyl alcohol (25:24:1). The 8209 bp-long *SlABCG42*
875 (*Solyc06g065670*) gene was amplified from genomic this DNA using the primers
876 SlABCG42 attB1 F and SlABCG42 attB2 R, and recombined into pDONR 207 to
877 generate *pENTRY L1-SlABCG42-L2*. To generate *pAtABCG32::GFP-SlABCG42,* the
878 CaMV35S promoter was removed from pMDC43 [63] by restriction enzyme digestion
879 with HindIII and KpnI. A 2043 bp-long fragment of the native *ABCG32/PEC1* promoter
880 was amplified using the primers pAtABCG32+HindIII F and pAtABCG32+KpnI R and
881 cloned into pMDC43, creating the plasmid pMDC43_*pABCG32::GFP*. *pENTRY L1-*
882 *SlABCG42-L2* was recombined with the destination vector *pAtABCG32::GFP* giving the
883 final construct *pAtABCG32::GFP-SlABCG42* for the expression of a SlABCG42 fusion
884 protein having eGFP at the N-terminus. *pAtABCG32::GFP* was used as control.
885 Constructs were transformed in *Agrobacterium tumefaciens* (GV3101mp90) and then
886 into *Arabidopsis thaliana* accession *pec1-2* using the floral dip method [64]. Shortly,
887 inflorescences were dipped into a 5% sucrose/0.05% Silwet L-77 solution containing
888 *Agrobacterium* for 30 s and kept under high humidity for 24 h. Transformed seeds were

889 selected based on their resistance to 150 µg mL^{-1} of hygromycin on ½ Murashige and
890 Skoog (MS) medium.

891 Constructs for the heterologous expression of the ABCG transporters in *N.*
892 *benthamiana:* The plasmid for the expression of YFP-AtABCG11 under the control of
893 the CaMV 35S promoter (pEARLYGATE_p35S::YFP-WBC11) was kindly provided by
894 Lacey Samuels [25]. The pMDC43_*p35S::GFP-AtABCG32* plasmid for the expression
895 eGFP-AtABCG32 was previously described [31]. To express GFP-SlABCG42 under
896 the control of the CaMV35S promoter, the *pENTRY L1-SlABCG42-L2* was recombined
897 with pMDC43 resulting in pMDC43_p*35S::GFP-SlABCG42.* The mutated versions of
898 pMDC43_p*35S::GFP-AtABCG32* and pMDC43_p*35S::GFP-SlABCG42* for the
899 expression of GFP-AtABCG32-M and GFP-SlABCG42-M were generated using the Q5
900 (r) Site-Directed Mutagenesis kit (NEB) following the manufacturer instructions and
901 were named pMDC43_p*35S::GFP-AtABCG32*_M and pMDC43_p*35S::GFP-*
902 *SlABCG42*_M, respectively. Primers were designed by using the NEBaseChanger™
903 tool for changing two nucleotides in the *AtABCG32* and *SlABCG42* sequences inducing
904 K174L and K165L mutations, respectively, in the Walker A1 motif of the transporters.
905 Constructs were transformed in *Agrobacterium tumefaciens* (GV3101 mp90). Leaves
906 of 4-weeks-old *N. benthamiana* plants were transfected following the protocol
907 described by Leuzinger et al., 2013 [65] : An Agrobacterium solution was prepared at
908 a final OD_{600} of 0.8 for construct diluted in the AS medium (1M MES-KOH, pH 5.6; 3M
909 $MgCl_2$, 150mM acetosyringone). Co-infiltration with a vector encoding the silencing
910 suppressor P19 from the tomato bushy stunt virus [66] was performed for high level
911 target gene expression (final OD_{600} of 0.1). For co-localization with PIP2A-mCherry
912 construct pm-rk (ARBC stock number CD3-1007) was transformed in Agrobacterium
913 tumefaciens (GV3101 mp90) used at a final OD_{600} of 0.4-0.5 [43].

914 Constructs for *RNAi-dependent gene silencing of SlABCG36 and SlABCG42* tomato:
915 *S. lycopersicum* L. *SlABCG36* (*Solyc05g018510*) and *SlABCG42* (*Solyc06g065670*)
916 gene sequences were obtained from the annotation of the tomato genome (ITAG v2.4).
917 Silencing fragments were designed in sequences encoding the transmembrane
918 domains having for weak sequence homology to other ABCG genes by using the SGN
919 VIGS tool (https://vigs.solgenomics.net/). Fragments were amplified from *S.*
920 *lycopersicum cv* “Micro-Tom” leaf cDNA that was prepared as described below (gene
921 expression analysis). *pENTRY L1-fragSlABCG36-L2* was generated by cloning the 224

bp-fragment of *Solyc05g018510* resulting from a PCR reaction using the primers fragSlABCG36 F and fragSlABCG36 R into pDONR207. *pENTRY L1-fragSlABCG42-L2* was generated by cloning the 234bp fragment of the *Solyc06g065670* gene, that was generated by PCR reaction using the primers fragSlABCG42 F and fragSlABCG42 F in the pDONR207 vector. Both pENTRY plasmids were recombined with the destination vector pK7GWIWG2 [67] resulting in pK7GWIWG2-fragSlABCG36 and pK7GWIWG2-fragSlABCG42. Constructs were transformed in *Agrobacterium tumefaciens* (GV3101).

Transformation *of S. lycopersicum cv* Micro Tom was performed as described by Cardenas et al., 2019 [68]. Shortly, cotyledon explants were excised from 7-day-old *in vitro* grown tomato seedlings, and placed on co-cultivation medium (3% Glucose, 0.02% KH2PO4, 75 ug/mL DTT, 2ug/mL Zeatin, 1ug/mL IAA, 100uM acetosyringone) plus 3% GelRite and preincubated for 24 h at room temperature in the dark. Co-cultivation of the explants with the transformed *A. tumefaciens* strains (OD_{600} = 0.3) was carried out for 48 h under dark conditions in liquid co-cultivation medium. Explants were transferred to shoot induction medium: MS medium containing dithiothreitol (DTT - 75 µg mL^{-1}), Kanamycin (50 µg mL^{-1}), Zeatin (2 µg mL^{-1}), indole-3-acetic acid (IAA - 1 µg mL^{-1}), and Timentin (5000 µg mL^{-1}) for 2 to 3 weeks. Timentin was used to remove *Agrobacterium* from the explants. Once the explants developed callus, they were transferred to the shoot elongation medium containing DTT (75 µg mL^{-1}), Kanamycin (50 µg mL^{-1}), Zeatin (1 µg mL^{-1}), Zeatin riboside (1 µg mL^{-1}), IAA (1 µg mL^{-1}), and Timentin (250 µg mL^{-1}). Subsequently, well-developed shoots were excised and transferred to rooting medium containing Kanamycin (50 µg mL^{-1}), and Timentin (250 µg mL^{-1}). After 3-4 weeks, plantlets with roots were transplanted to sterile soil and covered to conserve humidity for a week when they were finally transferred to greenhouse conditions (16 h light/24°C and 8 h dark/20°C). Transgenic lines were selected by qPCR. Plants in the T3 generation were used for further analysis.

Gene expression analysis

Quantitative real time PCR was performed with three biological replicates from several tomato plants ($n \geq 4$) for each genotype. RNA isolation was performed from two 0.5 cm exocarp discs for each sample using the ReliaPrep™ RNA Miniprep Systems (Promega) following the guidelines of the manufacturer. RNA was reverse transcribed using the Moloney Murine Leukemia Virus Reverse Transcriptase RNase H

Minus, *Point Mutant* (M-*MLV RT*(H–)) (Promega). Quantitative real-time PCR was performed using 200 nM of the appropriated primers and the Select Master Mix (Applied Biosystems). Using the QuantStudio™ 3 Real-Time PCR System (Applied Biosystems) with the following parameters: UDG Activation at 50°C for 2 min, denaturation at 95°C for 2 min, 40 amplification cycles with a denaturation step at 95°C for 15 s, an annealing step at 60°C for 30 s and an amplification step at 72°C for 30 s. Data acquisition and analysis were done using the QuantStudio™ Software V1.3 (Applied Biosystems). *TIP41* (SGN-U321250) based on Expósito-Rodríguez et al. (2008) [69] was used as reference gene to calculate relative transcript expression using gene expression analysis. Primers for measuring silencing annealed outside the region of the fragment used for silencing to assure that only the endogenous gene is being measured. All primers are listed in Table S1B.

Transport assays

Transport assays were performed as previously described by Geisler et al., 2005 [62]. Leaves of 4-weeks-old *N. benthamiana* plants were agroinfiltrated with the following constructs: *35S::YFP-AtABCG11, 35S::GFP-AtABCG32, 35S::GFP-SlABCG42*, and the mutated versions *35S::GFP-AtABCG32-M, 35S::GFP-SlABCG42-M.* The *P19* silencing inhibitor (control) was always co-infiltrated. After four days protoplasts were prepared. Two radiolabelled substrates, i.e. one [^{3}H]-labelled and one [^{14}C]-labelled were added at this stage: [^{3}H]-10,16-diOH C16:0 2-glycerol and [^{14}C]-ω-OH C16:0, [^{14}C]-C16:0 DCA or [^{14}C]-indole-3-acetic acid (IAA; control) were added to the protoplast to yield a final concentration of 1 µM each. The mixture was incubated on ice for 15 min for substrate intake. External radioactivity was removed by separating protoplasts using a 50%/25%/5% Percoll gradient built from bottom to top: protoplasts in Percoll pH 6, 1 Volume, 1 Vol. Percoll 25%, 5 ml Percoll 5%. Protoplasts were recovered from the 25%/5% Percoll interphase. For the export experiment, protoplasts were diluted 1:3 with Betain buffer and incubated at 25°C. Aliquots of 70 µL were taken at 0, 5, 10, 15, and 20 min. Aliquots were centrifuged in a silicon oil gradient (50 µL 33% Percoll/ 200 µL silicon oil AR200) for 30 s at 9000 rpm, and supernatants were objected to scintillation counting. Indicated relative uptake was calculated as the radioactivity normalized to the first time point (0 min). Experiment were repeated at least four times, and data are presented as means with the standard error of the mean (SEM) of all technical replicates.

Microscopy studies

Confocal imaging:

Leaf discs of *N. benthamiana* were observed 2 or 3 days after agroinfiltration at the laser scanning confocal microscope, Zeiss LSM880 (Carl Zeiss, Germany) with setting parameters for the observation of YFP (λ_{ex}: 516; λ_{em}: 529), GFP (λ_{ex}: 475; λ_{em}: 503), mCherry (λ_{ex}: 587; λ_{em}: 610) and propidium iodide (PI) (λ_{ex}: 535; λ_{em}: 617) or with the Leica SP5 (Leica, Germany) with the setting parameters for GFP (λ_{ex}: 488; λ_{em}: 505-530) and for PI (λ_{ex} 488; λ_{em} 610 – 620). Leaf discs were incubated for 20 min in PI (20µg/ml) and washed 10 min in water before observation to visualize the cell wall.

Light microscopy: Three tomato fruits of each line and developmental stage were harvested and small equatorial pericarp pieces of each fruit were fixed in a formaldehyde, acetic acid and ethanol solution (FAA solution, 1:1:18). Serial dehydration steps were performed for 1h each in ethanol (50% to 100%). Pieces were embedded in the commercial resin Technovit 7100 following the manufacturer instructions. Samples were cross-sectioned into 8 µm thick slices using a Leica (Wetzlar, Germany) microtome (RM2125). Sudan IV was used to distinctively stain the cuticle using the protocol described by Buda et al. (2009) [70]. Sudan IV stock solution (0.1% w/v in isopropyl alcohol) was diluted 3:2 with distilled water, mixed well, allowed to sit at room temperature for 30 min, and filtered through a Whatman filter paper to remove precipitates. Sections were incubated in the Sudan IV solution for 10 min, and subsequently rinsed first with 50% isopropyl alcohol and distilled water. Slices were mounted in distilled water with a cover slip, and viewed immediately. A minimum of five slices per sample were inspected under light microscope (DM5500, Carl Zeiss). Microphotographs were taken with a Nikon camera (DXM1200) coupled to the light microscope. Cuticle area was estimated from a minimum of 15 measurements using an image capture analysis program (Fiji v 2.0.0) using a square area of 250 x 70 µm [71].

Transmission electron microscopy (TEM): Fully open flowers of *A. thaliana* and 1.2 mm discs of the tomato fruits were fixed 2.5% glutaraldehyde solution in 0.1M phosphate buffer pH 7.4 (PB) for 2 h at room temperature (RT). They were rinsed three times for 5 min in PB buffer and post-fixed in a fresh mixture of osmium tetroxide 1% (EMS) with 1.5% potassium ferrocyanide in PB buffer for 2 h at RT. The samples were then washed two times in distilled water and dehydrated in acetone solution at graded concentrations

(30%–40 min; 50%–40 min; 70%–40 min; 100%–3 x 1 h). The infiltration with Spurr resin at 33% in acetone for 12 h, Spurr 66% in acetone for 12 h, Spurr 100% for 1h, Spurr 100% twice for 8 h. The *Arabidopsis* flowers were then dissected in the resin under a binocular. Petals discs were placed in molds filled with resin and then polymerized for 48 h at 60°C. Ultrathin sections of 60 nm thick were cut on a Leica Ultracut (Leica Mikrosysteme GmbH), picked up on a copper slot grid 2x1 mm (EMS) coated with a polystyrene film (Sigma Aldrich). Sections were post-stained with 4% uranyl acetate in distilled water for 10 min, rinsed several times with distilled water followed by Reynolds lead citrate in water for 10 min and rinsed several times with distilled water. Micrographs were taken with a transmission electron microscope FEI CM100 (FEI, Eindhoven, The Netherlands) at an acceleration voltage of 80 kV with a TVIPS TemCamF416 digital camera (TVIPS GmbH) using the software EM-MENU 4.0 (TVIPS GmbH).

Scanning electron microscopy: tomato fruit pieces were investigated by cryo-scanning electron microscopy directly without solvent treatment. For cryo-scanning electron microscopy, we used a Quorum system PP3000T (Quorum Technologies Ltd) attached to a Quanta 250 FEI scanning electron microscope (FEI Company). The tomato pieces were mounted on aluminum stubs using a mixture of Tissue-Tek and colloidal graphite, frozen in nitrogen slush at −210°C and then transferred to the preparation chamber of the Quorum system. The sample was freeze-dried at −80°C for 10 min, and then sputter-coated with platinum at 10 mA for 25 s. After transfer on the cryostage at −140°C in the scanning electron microscope, imaging was performed, at the tomato equatorial area, at 10 keV using an Everhart-Thornley electron detector.

Scanning and transmission electron micrographs were taken from at least 3 different fruits of for minimally two different plants per line.

Isolation of tomato fruit cuticles

Cuticles were isolated from the fruits of wild-type and transgenic lines by incubating tomato halves in 2% pectinase and 0.2% cellulase in 0.02 M citrate buffer pH 3.7. Incubation was performed at 37°C for at least 2 weeks with regular changes of the enzymatic mixture [72].

Chemical analyses

Cutin analysis: The protocol for the determination of ester-bond lipids previously described in Li-Beisson et al., 2013 [73] was adapted. For the analysis of floral cutin of Arabidopsis 20 fully open flowers from four to six plants were collected. For the analysis tomato cutin four discs of isolated cuticles (1 cm diameter) from 8 tomatoes coming from two different plants per line were used. Four samples per line and per stage were analyzed. All plant samples were delipidated by an initial incubation in 7 mL isopropanol /0.01% butylated hydroxytoluene (BHT) for 10 min at 85°C and then subsequent washes in methanol:chloroform with 0.01% BHT (1:2, 1:1, 2:1, respectively), finishing by 24 h in 100% methanol/0.01% BHT. Samples were then dry under a gentle stream of nitrogen at 30°C and kept for 3 days in a desiccator. Depolymerization was performed by base catalyzed transesterification in dry methanol containing 15% (v/v) methyl acetate and 6% (v/v) sodium methoxide, and ω-pentadecalactone (2.5 µg) and methyl heptadecanoate (5 µg) were added to the reaction medium as an internal standard. Reactions was incubated for 2 h at 60°C. 3.5 mL dichloromethane, 0.7 mL glacial acetic acid and 1 mL 0.9% NaCl (w/v) Tris 100 mM pH 8.0 were added to each sample and subsequently vortexed for 20 s. After centrifugation (1500 g for 2 min), the organic phase was collected, washed with 2 mL of 0.9% NaCl, and dried over sodium sulfate. The organic phase was then recovered and concentrated under a stream of nitrogen. Monomers were derivatized by acetylation using 20 µL of anhydrous pyridine and 20 µL of acetic anhydride and incubated at 60°C for 2h. Tomato fruit samples were injected in split mode (30:1), while Arabidopsis samples were infected split-less out of hexane into a gas chromatograph coupled to a mass spectrometer and a flame ionization detector (Agilent 6890N GC Network systems) equipped with a HP-5 capillary column (30 m, 0.32 mm ID, 0.25 µm film thickness, J&W Scientific) (temperature program: 2 min at 50°C, increment of 20°C/min to 140°C, of 3°C/min 310°C, held for 10 min). Peaks quantified on the basis of their FID ion current.

Wax analysis: Wax components were analyzed by submerging the freshly peeled discs in 7 mL of chloroform for 30 s twice, and then derivatized by sylation, with BFTSA/pyridine (1:1) at 70°C for 1 h. Samples were injected out of chloroform in a gas chromatograph coupled to a mass spectrometer and a flame ionization detector (Agilent 6890N GC Network systems) on a HP-1 column (30 m, 0.32 mm ID, 1 µm film thickness, (Agilent)) (temperature program: 50°C for 2 min, raise by 40°C min–1 to

200°C, held for 2 min at 200°C, raised by 3°C min–1 to 320°C, and held for 30 min at 320°C). Peaks were quantified on the basis of their FID ion current.

Glycerol determination in cutin: Glycerol was released by mild methanolysis using the protocol described by Graça et al., 2002 [74] with slight modifications. Isolated cutin slices (3 mm x 3 mm) were stirred at room temperature in a mixture of 50 mM sodium methoxide in dry methanol with the internal standard 1,2,4-butanetriol [75]. After 20 h, the extract was dried with a nitrogen flow, silylated with 1% N, O-bis(trimethylsilyl)trifluoroacetamide/trimethyl chlorosilane, and analyzed by gas chromatography-flame ionization detection.

Ester-linkage pattern of 10,16-dihydroxy hexadecenoic acid in cutin: Free hydroxy groups were derivatized by benzyl etherification by a procedure adapted from a procedure developed for organic alcohols [76]. Isolated dewaxed cutins were mixed with 15 µg of 2-benzyloxy-1-methylpyridinium triflate and 1.68 µg of magnesium oxide in 1 µL of trifluorotoluene in a 7 mL screw-capped glass tube at 90°C overnight. Cutin was then washed extensively with dichloromethane and dried. By comparing different sizes of cutin samples and cutin powders, verification that the same amount of derivatized cutin monomer was performed, indicating that cutin diffusion barriers did not hinder the reaction.

Cuticle permeability assays

For studying the permeability of the cuticle of *Arabidopsis* leaves, a drop (5 µL) of an aqueous solution of 0.05% w/v toluidine blue (TB)/0.001% Tween 20 was applied on expanding leaves for 45 min. Fully open inflorescences were dipped in the same TB solution for 45 min. TB was washed away with running water.

For water loss assays, at least 10 isolated cuticles and dewaxed cuticles (cutins) of tomato fruits were mounted to stainless steel transpiration chambers as described previously [77] with the exception that the exposed area was 28 mm^2 and not 1.13 cm^2. Permeances for water (m s^{-1}) were calculated from the slopes of regression lines fitted to the plots water amount lost versus time using the equation P = water loss / (time x exposed area x driving force). Since humidity outside the chamber was 0 the driving force corresponded to pure water in the chamber, which is 1 g cm^{-3}.

QUANTIFICATION AND STATISTICAL ANALYSIS

For the chemical analyses of the cutin and wax composition, the glycerol amount, the gene expression, cuticle area and water permeability measurements, presented values are the mean ± standard deviation. Two-way ANOVA with Tukey HSD multiple comparison, $P<0.05$ were performed to highlight differences among the genotypes. For the transport assays, data are represented as mean ± SEM; multiple t-tests followed by Holm-Sidak multiple comparisons correction were performed to highlight the differences between Control and other constructs. ns: not significant. Letters were assigned to differently significant groups; a = $p < 0.001$ and b = $p < 0.05$. Number of repetitions and replicates are mentioned for each experiment in the method details.

References

1. Riederer, M. (2006). Introduction: biology of the plant cuticle. In Biology of the Plant Cuticle, M. Riederer and C. Müller, eds. (Oxford: Blackwell Publishing), pp. 1-10.
2. Kosma, D.K., Parsons, E.P., Isaacson, T., Lu, S.Y., Rose, J.K.C., and Jenks, M.A. (2010). Fruit cuticle lipid composition during development in tomato ripening mutants. Physiologia Plantarum *139*, 107-117.
3. Girard, A.-L., Mounet, F., Lemaire-Chamley, M., Gaillard, C., Elmorjani, K., Vivancos, J., Runavot, J.-L., Quemener, B., Petit, J., Germain, V., et al. (2012). Tomato GDSL1 Is required for cutin deposition in the fruit cuticle. The Plant Cell *24*, 3119-3134.
4. Mazurek, S., Garroum, I., Daraspe, J., De Bellis, D., Olsson, V., Mucciolo, A., Butenko, M.A., Humbel, B.M., and Nawrath, C. (2017). Connecting the Molecular Structure of Cutin to Ultrastructure and Physical Properties of the Cuticle in Petals of Arabidopsis. Plant Physiology *173*, 1146-1163.
5. Fich, E.A., Segerson, N.A., and Rose, J.K.C. (2016). The Plant Polyester Cutin: Biosynthesis, Structure, and Biological Roles. In Annual Review of Plant Biology, Vol 67, Volume 67, S.S. Merchant, ed., pp. 207-233.
6. Li, Y.H., Beisson, F., Koo, A.J.K., Molina, I., Pollard, M., and Ohlrogge, J. (2007). Identification of acyltransferases required for cutin biosynthesis and production of cutin with suberin-like monomers. Proceedings of the National Academy of Sciences of the United States of America *104*, 18339-18344.
7. Li-Beisson, Y., Pollard, M., Sauveplane, V., Pinot, F., Ohlrogge, J., and Beisson, F. (2009). Nanoridges that characterize the surface morphology of flowers require the synthesis of cutin polyester. Proceedings of the National Academy of Sciences of the United States of America *106*, 22008-22013.
8. Yang, W., Pollard, M., Li-Beisson, Y., Beisson, F., Feig, M., and Ohlrogge, J. (2010). A distinct type of glycerol-3-phosphate acyltransferase with *sn-2* preference and phosphatase activity producing 2-monoacylglycerol. Proceedings of the National Academy of Sciences of the United States of America *107*, 12040-12045.
9. Rautengarten, C., Ebert, B., Ouellet, M., Nafisi, M., Baidoo, E.E.K., Benke, P., Stranne, M., Mukhopadhyay, A., Keasling, J.D., Sakuragi, Y., et al. (2012). The Arabidopsis *DEFICIENT IN CUTIN FERULATE* (*DCF*) encodes a transferase required for feruloylation of ω-hydroxyfatty acids in cutin polyester. Plant Physiology *158*, 654-665.

10. Panikashvili, D., Shi, J.X., Schreiber, L., and Aharoni, A. (2009). The Arabidopsis *DCR* encoding a soluble BAHD acyltransferase is required for cutin polyester formation and seed hydration properties. Plant Physiology *151*, 1773-1789.
11. Dominguez, E., Heredia-Guerrero, J.A., and Heredia, A. (2015). Plant cutin genesis: unanswered questions. Trends in Plant Science *20*, 551-558.
12. Philippe, G., Gaillard, C., Petit, J., Geneix, N., Dalgalarrondo, M., Bres, C., Mauxion, J.-P., Franke, R., Rothan, C., Schreiber, L., et al. (2016). Ester Cross-Link Profiling of the Cutin Polymer of Wild-Type and Cutin Synthase Tomato Mutants Highlights Different Mechanisms of Polymerization. Plant Physiology *170*, 807-820.
13. Yeats, T.H., Huang, W., Chatterjee, S., Viart, H.M.F., Clausen, M.H., Stark, R.E., and Rose, J.K.C. (2014). Tomato Cutin Deficient 1 (CD1) and putative orthologs comprise an ancient family of cutin synthase-like (CUS) proteins that are conserved among land plants. Plant Journal *77*, 667-675.
14. Yeats, T.H., Martin, L.B.B., Viart, H.M.F., Isaacson, T., He, Y.H., Zhao, L.X., Matas, A.J., Buda, G.J., Domozych, D.S., Clausen, M.H., et al. (2012). The identification of cutin synthase: Formation of the plant polyester cutin. Nature Chemical Biology *8*, 609-611.
15. Shi, J.X., Malitsky, S., De Oliveira, S., Branigan, C., Franke, R.B., Schreiber, L., and Aharoni, A. (2011). *SHINE* transcription factors act redundantly to pattern the archetypal surface of Arabidopsis flower organs. PLoS Genet *7*, e1001388.
16. Kurdyukov, S., Faust, A., Nawrath, C., Bär, S., Voisin, D., Franke, R., Schreiber, L., Saedler, H., Métraux, J.-P., and Yephremov, A. (2006). The epidermis-specific extracellular BODYGUARD controls cuticle development and morphogenesis in Arabidopsis. Plant Cell *18*, 321-339.
17. Jakobson, L., Lindgren, L.O., Verdier, G., Laanemets, K., Brosche, M., Beisson, F., and Kollist, H. (2016). BODYGUARD is required for the biosynthesis of cutin in Arabidopsis. New Phytologist *211*, 614-626.
18. Guzman-Puyol, S., Benitez, J.J., Dominguez, E., Bayer, I.S., Cingolani, R., Athanassiou, A., Heredia, A., and Heredia-Guerrero, J.A. (2015). Pectin-Lipid Self-Assembly: Influence on the Formation of Polyhydroxy Fatty Acids Nanoparticles. Plos One *10*.
19. Do, T.H.T., Martinoia, E., and Lee, Y. (2018). Functions of ABC transporters in plant growth and development. Current Opinion in Plant Biology *41*, 32-38.
20. Bird, D.A. (2008). The role of ABC transporters in cuticular lipid secretion. Plant Science *174*, 563-569.
21. Verrier, P.J., Bird, D., Burla, B., Dassa, E., Forestier, C., Geisler, M., Klein, M., Kolukisaoglu, U., Lee, Y., Martinoia, E., et al. (2008). Plant ABC proteins--a unified nomenclature and updated inventory. Trends Plant Sci *13*, 151-159.
22. Verrier, P.J., Bird, D., Buria, B., Dassa, E., Forestier, C., Geisler, M., Klein, M., Kolukisaoglu, U., Lee, Y., Martinoia, E., et al. (2008). Plant ABC proteins - a unified nomenclature and updated inventory. Trends in Plant Science *13*, 151-159.
23. Andolfo, G., Ruocco, M., Di Donato, A., Frusciante, L., Lorito, M., Scala, F., and Ercolano, M.R. (2015). Genetic variability and evolutionary diversification of membrane ABC transporters in plants. Bmc Plant Biology *15*, 15.
24. Hwang, J.U., Song, W.Y., Hong, D., Ko, D., Yamaoka, Y., Jang, S., Yim, S., Lee, E., Khare, D., Kim, K., et al. (2016). Plant ABC Transporters Enable Many Unique Aspects of a Terrestrial Plant's Lifestyle. Molecular Plant *9*, 338-355.

25. Bird, D., Beisson, F., Brigham, A., Shin, J., Greer, S., Jetter, R., Kunst, L., Wu, X.W., Yephremov, A., and Samuels, L. (2007). Characterization of Arabidopsis ABCG11/WBC11, an ATP binding cassette (ABC) transporter that is required for cuticular lipid secretion. Plant Journal *52*, 485-498.
26. McFarlane, H.E., Shin, J.J.H., Bird, D.A., and Samuels, A.L. (2010). Arabidopsis ABCG Transporters, Which Are Required for Export of Diverse Cuticular Lipids, Dimerize in Different Combinations. Plant Cell *22*, 3066-3075.
27. Luo, B., Xue, X.Y., Hu, W.L., Wang, L.J., and Chen, X.Y. (2007). An ABC transporter gene of *Arabidopsis thaliana*, *AtWBC11*, is involved in cuticle development and prevention of organ fusion. Plant and Cell Physiology *48*, 1790-1802.
28. Panikashvili, D., Savaldi-Goldstein, S., Mandel, T., Yifhar, T., Franke, R.B., Hofer, R., Schreiber, L., Chory, J., and Aharoni, A. (2007). The Arabidopsis DESPERADO/AtWBC11 transporter is required for cutin and wax secretion. Plant Physiology *145*, 1345-1360.
29. Panikashvili, D., Shi, J.X., Schreiber, L., and Aharoni, A. (2011). The Arabidopsis ABCG13 transporter is required for flower cuticle secretion and patterning of the petal epidermis. New Phytologist *190*, 113-124.
30. Philippe, G., Sørensen, I., Jiao, C., Sun, X., Fei, Z., Domozych, D.S., and Rose, J.K. (2020). Cutin and suberin: assembly and origins of specialized lipidic cell wall scaffolds. Current Opinion in Plant Biology *55*, 11-20.
31. Bessire, M., Borel, S., Fabre, G., Carraca, L., Efremova, N., Yephremov, A., Cao, Y., Jetter, R., Jacquat, A.C., Metraux, J.P., et al. (2011). A member of the PLEIOTROPIC DRUG RESISTANCE family of ATP binding cassette transporters is required for the formation of a functional cuticle in Arabidopsis. Plant Cell *23*, 1958-1970.
32. Fabre, G., Garroum, I., Mazurek, S., Daraspe, J., Mucciolo, A., Sankar, M., Humbel, B.M., and Nawrath, C. (2016). The ABCG transporter PEC1/ABCG32 is required for the formation of the developing leaf cuticle in Arabidopsis. New Phytologist *209*, 192-201.
33. Chen, G.X., Komatsuda, T., Ma, J.F., Nawrath, C., Pourkheirandish, M., Tagiri, A., Hu, Y.G., Sameri, M., Li, X.R., Zhao, X., et al. (2011). An ATP-binding cassette subfamily G full transporter is essential for the retention of leaf water in both wild barley and rice. Proceedings of the National Academy of Sciences of the United States of America *108*, 12354-12359.
34. Garroum, I., Bidzinski, P., Daraspe, J., Mucciolo, A., Humbel, B.M., Morel, J.B., and Nawrath, C. (2016). Cuticular Defects in Oryza sativa ATP-binding Cassette Transporter G31 Mutant Plants Cause Dwarfism, Elevated Defense Responses and Pathogen Resistance. Plant and Cell Physiology *57*, 1179-1188.
35. Ofori, P.A., Mizuno, A., Suzuki, M., Martinoia, E., Reuscher, S., Aoki, K., Shibata, D., Otagaki, S., Matsumoto, S., and Shiratake, K. (2018). Genome-wide analysis of ATP binding cassette (ABC) transporters in tomato. Plos One *13*, 26.
36. Lashbrooke, J., Adato, A., Lotan, O., Alkan, N., Tsimbalist, T., Rechav, K., Fernandez-Moreno, J.P., Widemann, E., Grausem, B., Pinot, F., et al. (2015). The Tomato MIXTA-Like Transcription Factor Coordinates Fruit Epidermis Conical Cell Development and Cuticular Lipid Biosynthesis and Assembly. Plant Physiology *169*, 2553-2571.
37. Fernandez-Pozo, N., Zheng, Y., Snyder, S.I., Nicolas, P., Shinozaki, Y., Fei, Z.J., Catala, C., Giovannoni, J.J., Rose, J.K.C., and Mueller, L.A. (2017). The Tomato Expression Atlas. Bioinformatics *33*, 2397-2398.

38. Cui, L.P., Qiu, Z.K., Wang, Z.R., Gao, J.C., Guo, Y.M., Huang, Z.J., Du, Y.C., and Wang, X.X. (2017). Fine Mapping of a Gene (ER4.1) that Causes Epidermal Reticulation of Tomato Fruit and Characterization of the Associated Transcriptome. Frontiers in Plant Science *8*, 13.
39. Aryal, B., Huynh, J., Schneuwly, J., Siffert, A., Liu, J., Alejandro, S., Ludwig-Muller, J., Martinoia, E., and Geisler, M. (2019). ABCG36/PEN3/PDR8 Is an Exporter of the Auxin Precursor, Indole-3-Butyric Acid, and Involved in Auxin-Controlled Development. Frontiers in Plant Science *10*, 10.
40. Henrichs, S., Wang, B.J., Fukao, Y., Zhu, J.S., Charrier, L., Bailly, A., Oehring, S.C., Linnert, M., Weiwad, M., Endler, A., et al. (2012). Regulation of ABCB1/PGP1-catalysed auxin transport by linker phosphorylation. Embo Journal *31*, 2965-2980.
41. Ofori, P.A., Geisler, M., di Donato, M., Pengchao, H., Otagaki, S., Matsumoto, S., and Shiratake, K. (2018). Tomato ATP-Binding Cassette Transporter SlABCB4 Is Involved in Auxin Transport in the Developing Fruit. Plants-Basel *7*.
42. Frelet, A., and Klein, M. (2006). Insight in eukaryotic ABC transporter function by mutation analysis. Febs Letters *580*, 1064-1084.
43. Nelson, B.K., Cai, X., and Nebenfuhr, A. (2007). A multicolored set of in vivo organelle markers for co-localization studies in Arabidopsis and other plants. Plant Journal *51*, 1126-1136.
44. Zhou, Y.P., Sarker, U., Neumann, G., and Ludewig, U. (2019). The LaCEP1 peptide modulates cluster root morphology in Lupinus albus. Physiologia Plantarum *166*, 525-537.
45. Bianchetti, R.E., Lira, B.S., Monteiro, S.S., Demarco, D., Purgatto, E., Rothan, C., Rossi, M., and Freschi, L. (2018). Fruit-localized phytochromes regulate plastid biogenesis, starch synthesis, and carotenoid metabolism in tomato. Journal of Experimental Botany *69*, 3573-3586.
46. Shi, J.X., Adato, A., Alkan, N., He, Y.H., Lashbrooke, J., Matas, A.J., Meir, S., Malitsky, S., Isaacson, T., Prusky, D., et al. (2013). The tomato SlSHINE3 transcription factor regulates fruit cuticle formation and epidermal patterning. New Phytologist *197*, 468-480.
47. Isaacson, T., Kosma, D.K., Matas, A.J., Buda, G.J., He, Y.H., Yu, B.W., Pravitasari, A., Batteas, J.D., Stark, R.E., Jenks, M.A., et al. (2009). Cutin deficiency in the tomato fruit cuticle consistently affects resistance to microbial infection and biomechanical properties, but not transpirational water loss. Plant Journal *60*, 363-377.
48. Schreiber, L., and Schönherr, J. (2009). Water and solute Permeability of Plant Cuticles, (Springer Berlin Heidelberg).
49. Chen, G., Komatsuda, T., Ma, J.F., Nawrath, C., Pourkheirandish, M., Tagiri, A., Hu, Y.-G., Sameri, M., Li, X., Zhao, X., et al. (2011). An ATP-binding cassette subfamily G full transporter is essential for the retention of leaf water in both wild barley and rice. Proceedings of the National Academy of Sciences of the United States of America *108*, 12354-12359.
50. Petit, J., Bres, C., Mauxion, J.P., Tai, F.W.J., Martin, L.B.B., Fich, E.A., Joubes, J., Rose, J.K.C., Domergue, F., and Rothan, C. (2016). The Glycerol-3-Phosphate Acyltransferase GPAT6 from Tomato Plays a Central Role in Fruit Cutin Biosynthesis. Plant Physiology *171*, 894-913.
51. Hurlock, A.K., Roston, R.L., Wang, K., and Benning, C. (2014). Lipid Trafficking in Plant Cells. Traffic *15*, 915-932.

52. Nyathi, Y., Lousa, C.D.M., van Roermund, C.W., Wanders, R.J.A., Johnson, B., Baldwin, S.A., Theodoulou, F.L., and Baker, A. (2010). The Arabidopsis Peroxisomal ABC Transporter, Comatose, Complements the Saccharomyces cerevisiae pxa1 pxa2 Delta Mutant for Metabolism of Long-chain Fatty Acids and Exhibits Fatty Acyl-CoA-stimulated ATPase Activity. Journal of Biological Chemistry *285*, 29892-29902.
53. Yadav, V., Molina, I., Ranathunge, K., Castillo, I.Q., Rothstein, S.J., and Reed, J.W. (2014). ABCG Transporters Are Required for Suberin and Pollen Wall Extracellular Barriers in Arabidopsis. Plant Cell *26*, 3569-3588.
54. Landgraf, R., Smolka, U., Altmann, S., Eschen-Lippold, L., Senning, M., Sonnewald, S., Weigel, B., Frolova, N., Strehmel, N., Hause, G., et al. (2014). The ABC Transporter ABCG1 Is Required for Suberin Formation in Potato Tuber Periderm. Plant Cell *26*, 3403-3415.
55. Shanmugarajah, K., Linka, N., Grafe, K., Smits, S.H.J., Weber, A.P.M., Zeier, J., and Schmitt, L. (2019). ABCG1 contributes to suberin formation in Arabidopsis thaliana roots. Scientific Reports *9*.
56. Nawrath, C., Schreiber, L., Franke, R.B., Geldner, N., Reina-Pinto, J.J., and Kunst, L. (2013). Apoplastic diffusion barriers in Arabidopsis. The Arabidopsis book / American Society of Plant Biologists *11*, e0167-e0167.
57. Philippe, G., Geneix, N., Petit, J., Guillon, F., Sandt, C., Rothan, C., Lahaye, M., Marion, D., and Bakan, B. (2020). Assembly of tomato fruit cuticles: a cross-talk between the cutin polyester and cell wall polysaccharides. New Phytologist *226*, 809-822.
58. Segado, P., Dominguez, E., and Heredia, A. (2016). Ultrastructure of the Epidermal Cell Wall and Cuticle of Tomato Fruit (Solanum lycopersicum L.) during Development. Plant Physiology *170*, 935-946.
59. Petit, J., Bres, C., Just, D., Garcia, V., Mauxion, J.P., Marion, D., Bakan, B., Joubes, J., Domergue, F., and Rothan, C. (2014). Analyses of Tomato Fruit Brightness Mutants Uncover Both Cutin-Deficient and Cutin-Abundant Mutants and a New Hypomorphic Allele of GDSL Lipase. Plant Physiology *164*, 888-906.
60. Riederer, M., and Schreiber, L. (2001). Protecting against water loss: analysis of the barrier properties of plant cuticles. Journal of Experimental Botany *52*, 2023-2032.
61. Lai, C.P., Huang, L.M., Chen, L.F.O., Chan, M.T., and Shaw, J.F. (2017). Genome-wide analysis of GDSL-type esterases/lipases in Arabidopsis. Plant Molecular Biology *95*, 181-197.
62. Geisler, M., Blakeslee, J.J., Bouchard, R., Lee, O.R., Vincenzetti, V., Bandyopadhyay, A., Titapiwatanakun, B., Peer, W.A., Bailly, A., Richards, E.L., et al. (2005). Cellular efflux of auxin catalyzed by the Arabidopsis MDR/PGP transporter AtPGP1. Plant Journal *44*, 179-194.
63. Curtis, M.D., and Grossniklaus, U. (2003). A gateway cloning vector set for high-throughput functional analysis of genes in planta. Plant Physiology *133*, 462-469.
64. Clough, S.J., and Bent, A.F. (1998). Floral dip: a simplified method for Agrobacterium-mediated transformation of Arabidopsis thaliana. Plant Journal *16*, 735-743.
65. Leuzinger, K., Dent, M., Hurtado, J., Stahnke, J., Lai, H.F., Zhou, X.H., and Chen, Q. (2013). Efficient Agroinfiltration of Plants for High-level Transient Expression of Recombinant Proteins. Jove-Journal of Visualized Experiments.
66. Huang, Z., Chen, Q., Hjelm, B., Arntzen, C., and Mason, H. (2009). A DNA Replicon System for Rapid High-Level Production of Virus-Like Particles in Plants. Biotechnology and Bioengineering *103*, 706-714.

67. Karimi, M., Inze, D., and Depicker, A. (2002). GATEWAY((TM)) vectors for Agrobacterium-mediated plant transformation. Trends in Plant Science *7*, 193-195.
68. Cardenas, P.D., Sonawane, P.D., Heinig, U., Jozwiak, A., Panda, S., Abebie, B., Kazachkova, Y., Pliner, M., Unger, T., Wolf, D., et al. (2019). Pathways to defense metabolites and evading fruit bitterness in genus Solanum evolved through 2-oxoglutarate-dependent dioxygenases. Nature Communications *10*.
69. Exposito-Rodriguez, M., Borges, A.A., Borges-Perez, A., and Perez, J.A. (2008). Selection of internal control genes for quantitative real-time RT-PCR studies during tomato development process. Bmc Plant Biology *8*.
70. Buda, G.J., Isaacson, T., Matas, A.J., Paolillo, D.J., and Rose, J.K.C. (2009). Three-dimensional imaging of plant cuticle architecture using confocal scanning laser microscopy. Plant Journal *60*, 378-385.
71. Schindelin, J., Arganda-Carreras, I., Frise, E., Kaynig, V., Longair, M., Pietzsch, T., Preibisch, S., Rueden, C., Saalfeld, S., Schmid, B., et al. (2012). Fiji: an open-source platform for biological-image analysis. Nature Methods *9*, 676-682.
72. Schönherr, J., and Riederer, M. (1986). Plant cuticles sorb lipophilic compounds during enzymatic digestion. Plant, Cell and Environment *6*, 459-466.
73. Li-Beisson, Y., Shorrosh, B., Beisson, F., Andersson, M.X., Arondel, V., Bates, P.D., Baud, S., Bird, D., Debono, A., Durrett, T.P., et al. (2013). Acyl-lipid metabolism. The Arabidopsis book / American Society of Plant Biologists *11*, e0161-e0161.
74. Graça, J., Schreiber, L., Rodrigues, J., and Pereira, H. (2002). Glycerol and glyceryl esters of w-hydroxyacids in cutins. Phytochemistry *61*, 205-215.
75. Shen, Y.X., and Xu, Z.M. (2013). An improved GC-MS method in determining glycerol in different types of biological samples. Journal of Chromatography B-Analytical Technologies in the Biomedical and Life Sciences *930*, 36-40.
76. Lopez, S.S., and Dudley, G.B. (2008). Convenient method for preparing benzyl ethers and esters using 2-benzyloxypyridine. Beilstein Journal of Organic Chemistry *4*.
77. Schreiber, L., and Riederer, M. (1996). Ecophysiology of cuticular transpiration: Comparative investigation of cuticular water permeability of plant species from different habitats. Oecologia *107*, 426-432.

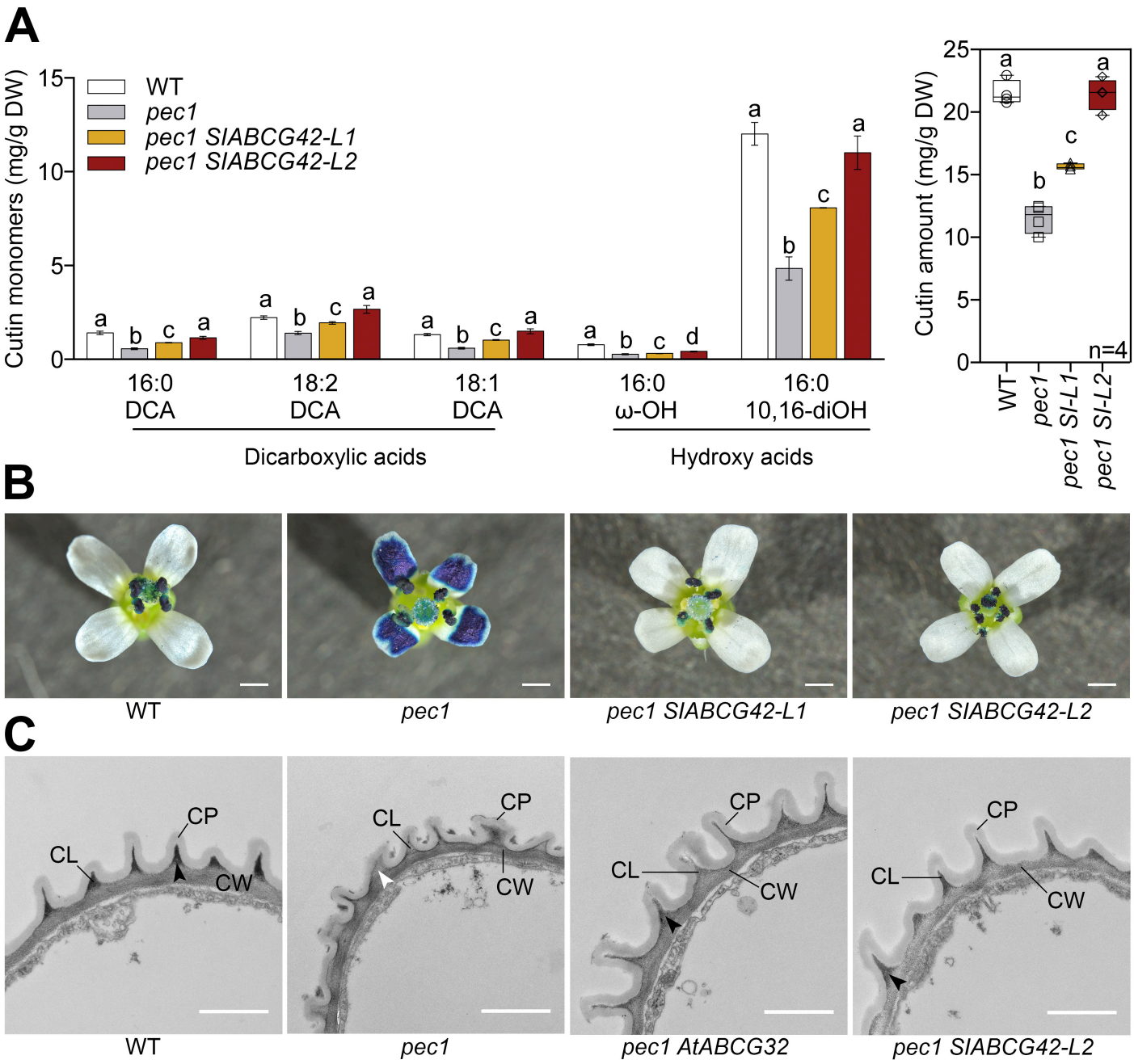

Figure 1. *SlABCG42* complements *pec1/atacbg32* mutant phenotypes

(A) Transgenic *pec1* lines expressing *SlABCG42* (*pec1 SlABCG42-L1* and *L2*) under the native *PEC1* promoter complement the monomer composition (left) as well as cutin amount (right) in flowers of the *pec1* mutant. Statistically significant differences are indicated by different letters (Two-way ANOVA, Tukey HSD multiple comparison, $P<0.05$, n=5). DW, dry weight. The analysis was performed twice with similar results and a representative data set is shown. Selected monomers are presented here. See Figure S2 for complete data set. **(B)** The cuticle permeability is restored in the *pec1 SlABCG42-L1* and *L2* lines. Toluidine blue (TB) staining is shown in flowers of different genotypes. Scale bar = 1 mm. **(C)** The structure of cuticle in petals in the *pec1 SlABCG42-L2* line is similar to WT, as seen in *pec1* complemented with *AtABCG32* (*pec1 AtABCG32*) [22]. Transmission electron micrographs (TEM) of petals in different genotypes highlighting the cuticular proper (CP), cuticular layer (CL) and cell wall (CW) of the cuticular ridges of the petal cuticle. Black arrows indicate electron dense areas in the cuticular layer; white arrows indicate the lack of this electron dense area. Scale bars represent 1 µm.

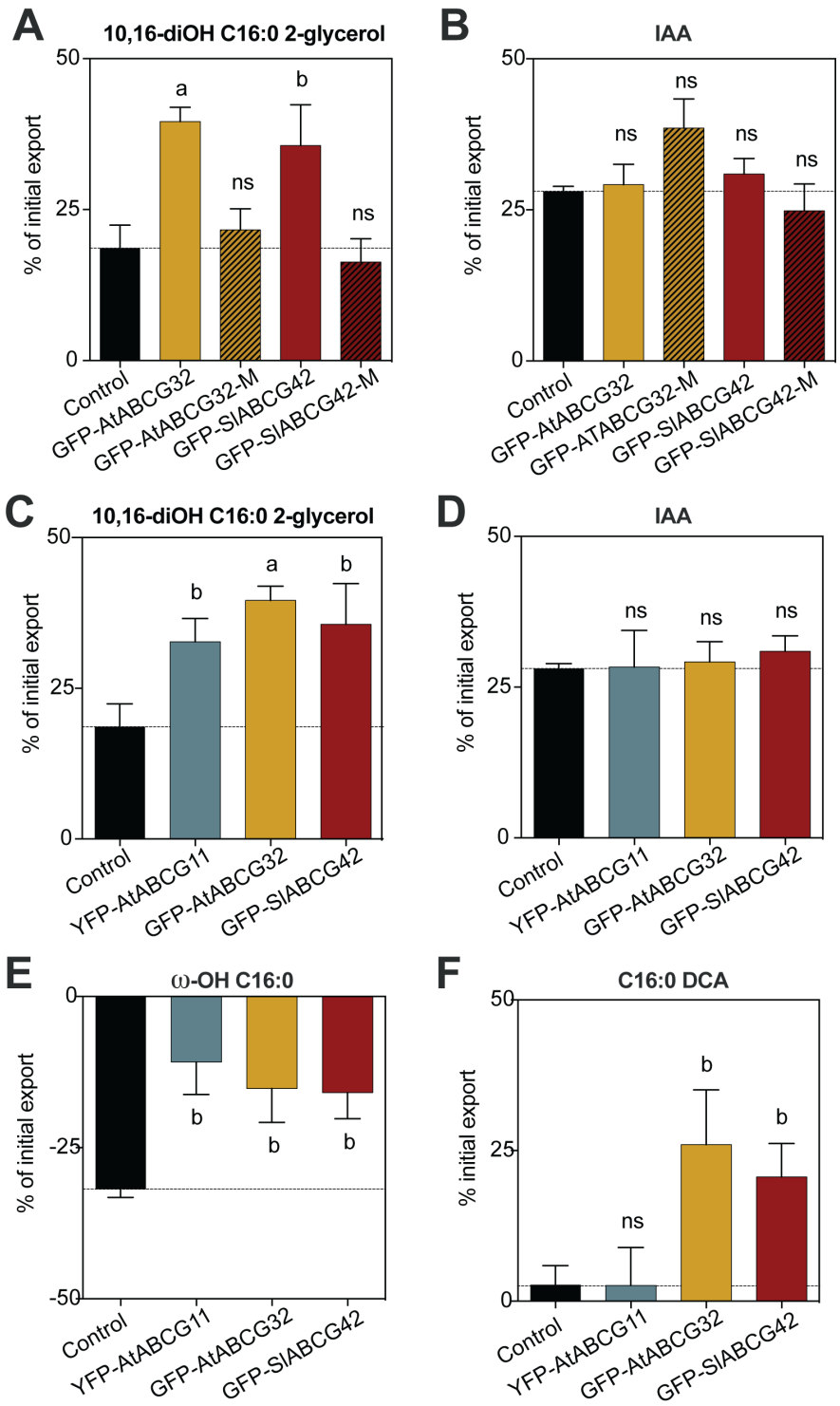

Figure 2. ABCG transporters required for cutin formation export C16:0 derivatives

(A, B) In transport assays using *N. benthamiana* protoplasts, AtABCG32 and SlABCG42 show transport activity with 10,16-diOH C16:0-2-glycerol in contrast to transport-incompetent versions mutated in the Walker A domain (AtABCG32-M and SlABCG42-M). Percentage of initial export across the plasma membrane of protoplasts expressing the empty vector (Control), GFP-AtABCG32, GFP-AtABCG32-M, GFP-SlABCG42, and GFP-SlABCG42-M with different substrates measured after 20 min are shown: (A) [^{3}H]-labeled 10, 16-diOH 16:0-2-glycerol; (B) [^{14}C]-labeled indole acetic acid (IAA) used as unrelated compound for comparison. **(C-F)** Heterologous expression of AtABCG32 and SlABCG42 as well as AtABCG11 in *N. benthamiana* protoplasts reveals export activity across the plasma membrane for 10,16 diOH C16:0 as well as ω-OH C16:0, while C16:0 DCA is only exported by AtABCG32 and SlABCG42. Percentage of initial export after 20 min of different substrates across the plasma membrane of protoplasts expressing the empty vector (Control), YFP-AtABCG11, GFP-AtABCG32 and GFP-SlABCG42. Three radiolabeled C16:0 substituted acids were used as substrates: (C) 10, 16-diOH 16:0-2-glycerol; (E) ω-OH C16:0; (F) C16:0 dicarboxylic acid (C16:0 DCA). (D) Radiolabeled indole acetic acid (IAA) was used as unrelated compound for comparison. Data represented as mean ± standard error of the mean; multiple t tests followed by Holm-Sidak multiple comparisons correction. Letters indicate significance groups; a = P<0.001 and b = P< 0.05; ns: not significant.

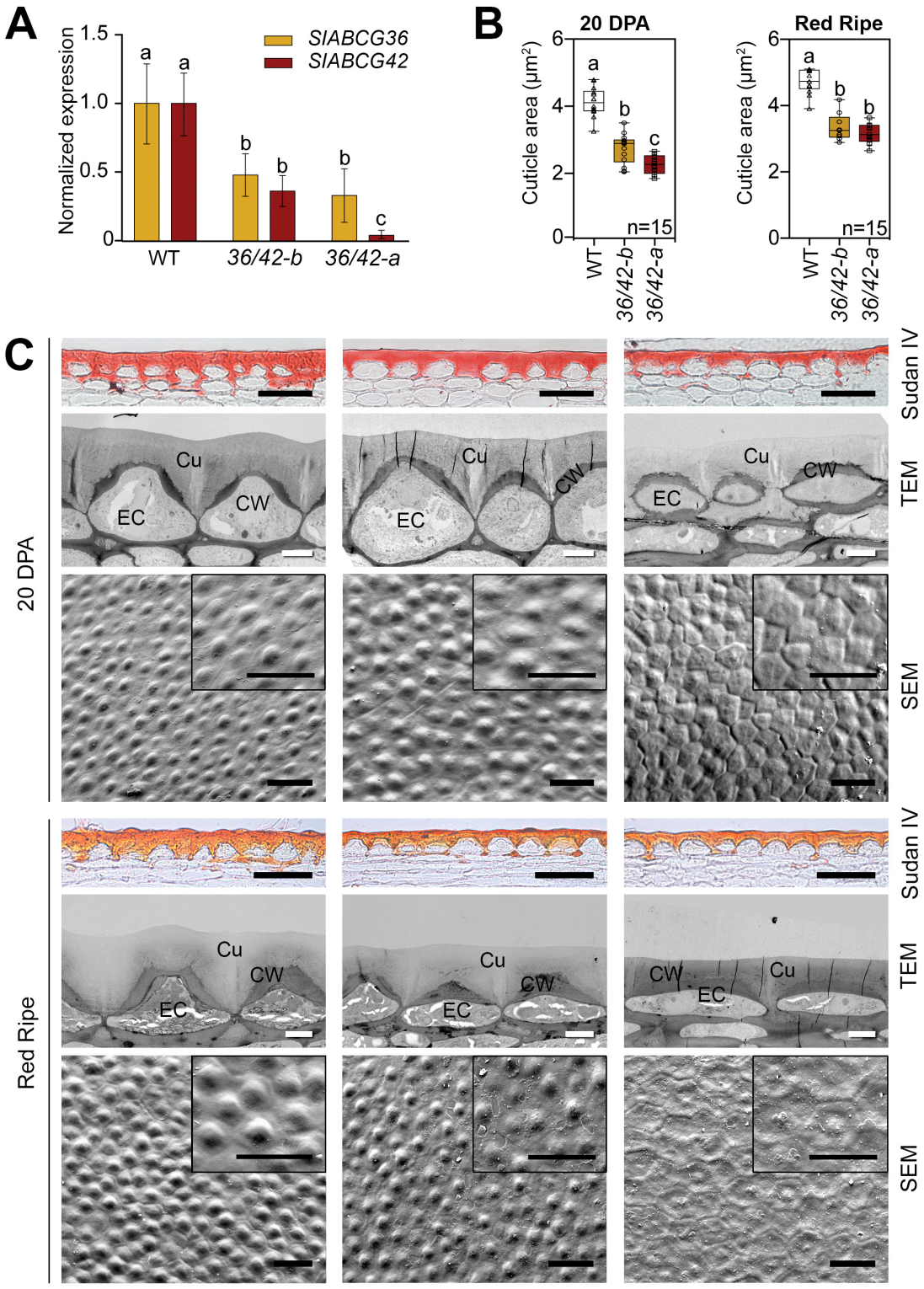

Figure 3. Reduced expression of *AtABCG32*-homologous genes and fruit cuticle formation in *slabcg36/42* plants

(A) Expression analysis of *SlABCG36* and *SlABCG42* in selected RNAi lines, i.e. *slabcg36/42-a* (*36/42-a*) and *slabcg36/42-b* (*36/42-b*) normalized to wild-type (WT) show significant differences between the RNAi lines in SlABCG42 expression as well as of both genes to WT. Real time-qPCR was performed with two biological replicates for 2 plants belonging to the same T3 line and three technical replicates by sample. Error bars represent SD. Analyses were performed with 10 DPA fruits. Statistically significant differences are indicated by different letters (Two-way ANOVA, Tukey HSD multiple comparison, $P<0.05$, $n=4$). The experiments were repeated twice with similar results. **(B)** and **(C)** Reduced cutinization and altered epidermal cell shape were revealed in fruits of *slabc36/42* plants. (B) Reduction of the cutinization of the tomato fruit cuticle as visible by Sudan IV staining (representative picture in (C) was quantified by measuring the Sudan stained area in 5 pictures of 250 µm x 70 µm in size. Statistically significant differences between cuticle areas are indicated by different letters (One-way ANOVA, Tukey HSD multiple comparison, $P < 0.05$, $n = 15$). (C) Cross sections of the fruit exocarp are shown in light microscopy and transmission electron microscopy (TEM) as well as of the fruit surface in cryo-scanning-electron microscopy (SEM). Two developmental stages are shown: 20 DPA and Ripe Red. Sudan IV staining revealed cuticle and cutinized cells of the first exocarp cell layer. WT, wild type. Transmission electron microscopy (TEM) images showing cuticular layer and epidermal cells structure. EC: epidermal cell, CW: cell wall, CL: Cuticular layer. White bars = 10 µm. Black bars = 50 µm.

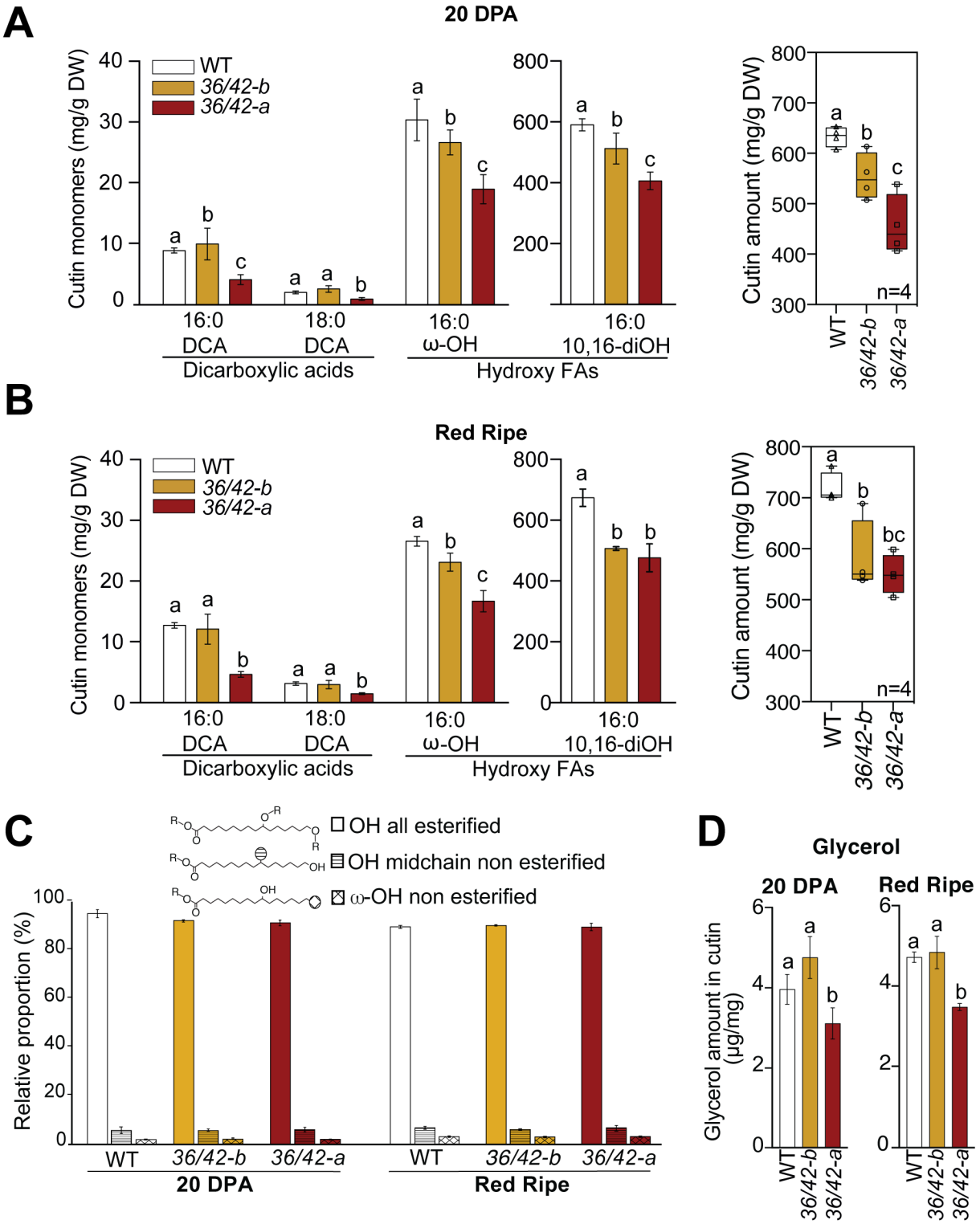

Figure 4. Reduced cutin deposition in *slabcg36/42 fruits*

The amount of the most abundant and selected minor cutin monomers (left) and the total cutin amount (right) present in isolated fruit cutins were quantified in 20 DPA-old **(A)** and in Red Ripe **(B)** fruits. Experiments were repeated at least twice and a representative set is shown here. Statistically significant differences between amount of cutin monomers and total cutin amounts are indicated by different letters (Two-way ANOVA, Tukey HSD multiple comparison, $P<0.05$, $n=4$). DW, dry weight. **(C)** Esterification levels of the different OH groups in 10,16-diOH C16:0 of cutin from fruits of wild-type (WT) and *slabcg36/42* lines are not different. Data were statistically analyzed by Two-way ANOVA, Tukey HSD multiple comparison, $P<0.05$, $n=5$. **(D)** Glycerol content in fruit cutin from the *slabcg36/42-a* plants is reduced. Statistically significant differences are indicated by different letters (Two-way ANOVA, Tukey HSD multiple comparison, $P<0.05$, $n=5$).

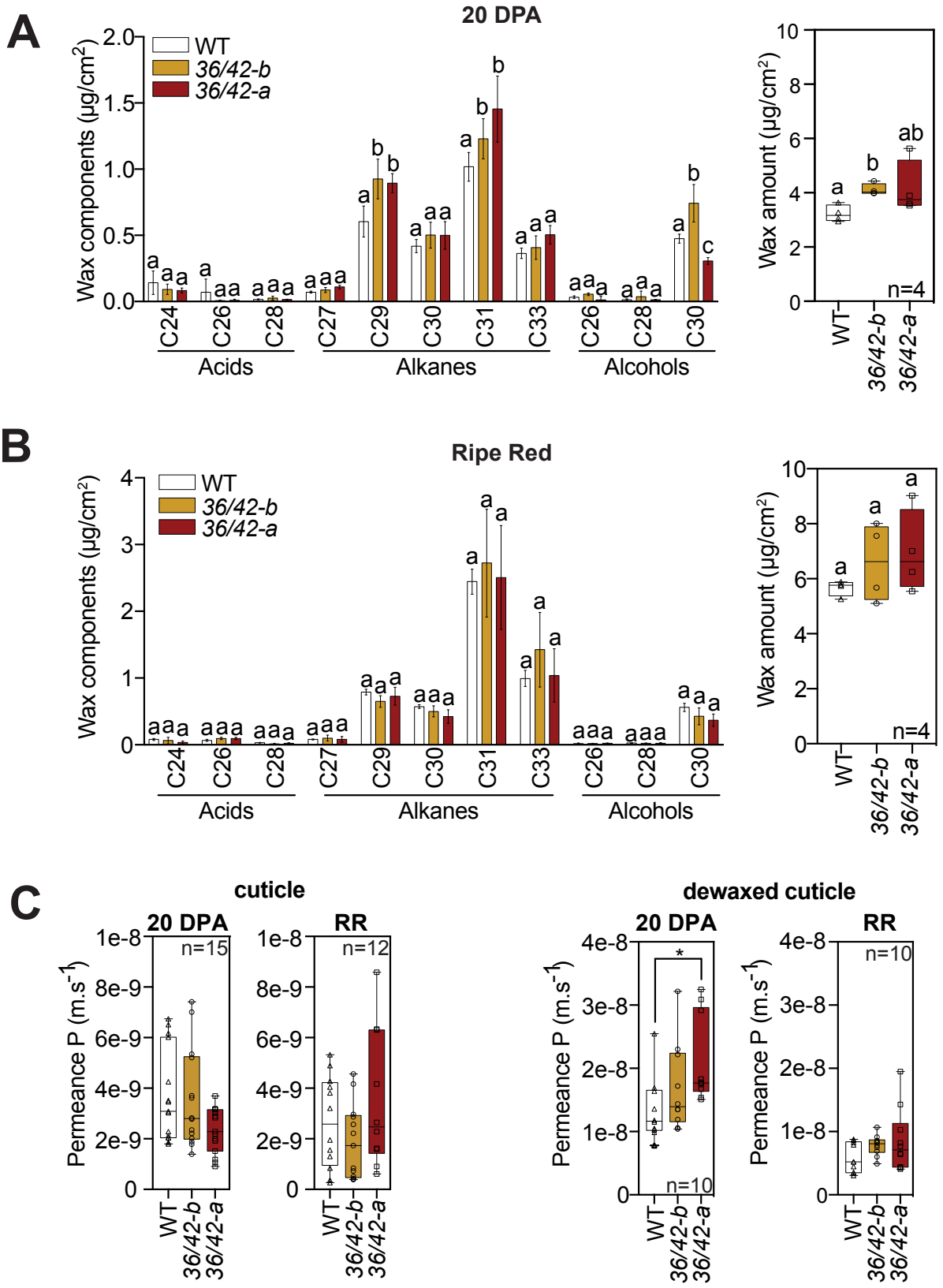

Figure 5. Wax deposition and water permeances of *slabcg36/42-RNAi* fruit cuticles

Increased deposition of wax components (left) and total wax (right) of *slabcg36/42* tomato fruits in different stages **(A)** 20 DPA and **(B)** Red Ripe fruits. Statistically significant differences are indicated by different letters (Two-way ANOVA, Tukey HSD multiple comparison, $P < 0.05$, $n = 5$). **(C)** Only dewaxed fruit cutins of *slabcg36/42* lines harvested at 20 DPA show increased permeability to water. The permeability of waxy and dewaxed cuticles was measured of 20 DPA and Red Ripe (RR) fruits. Student's *t*-test was used for assessing significant differences of wax components and water permeabilities when compared to WT (* = $p < 0.05$).

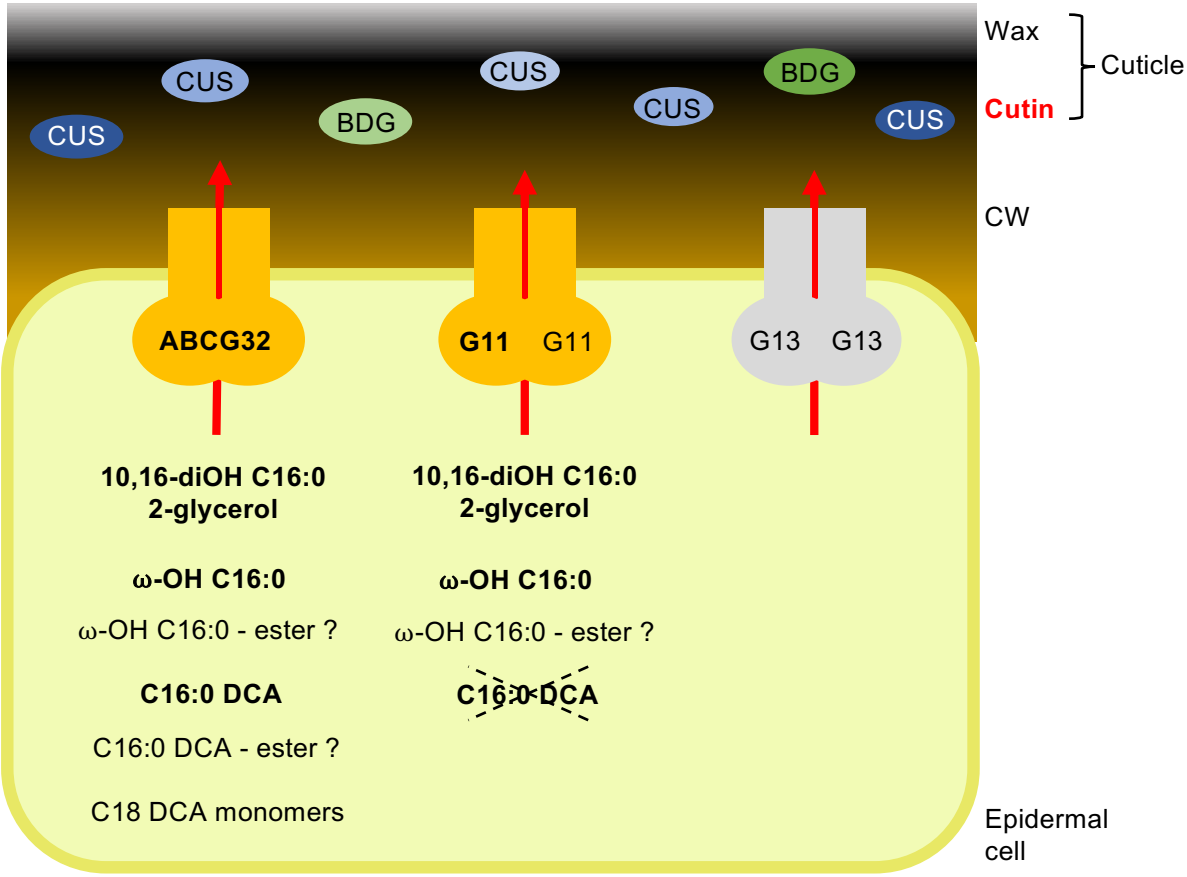
CUS
CUS
BDG
CUS
CUS
BDG
CUS
Wax
Cuticle
Cutin
CW
ABCG32
G11
G11
G13
G13
10,16-diOH C16:0
2-glycerol
10,16-diOH C16:0
2-glycerol
ω-OH C16:0
ω-OH C16:0 - ester ?
ω-OH C16:0
ω-OH C16:0 - ester ?
C16:0 DCA
C16:0 DCA
C16:0 DCA - ester ?
C18 DCA monomers
Epidermal
cell

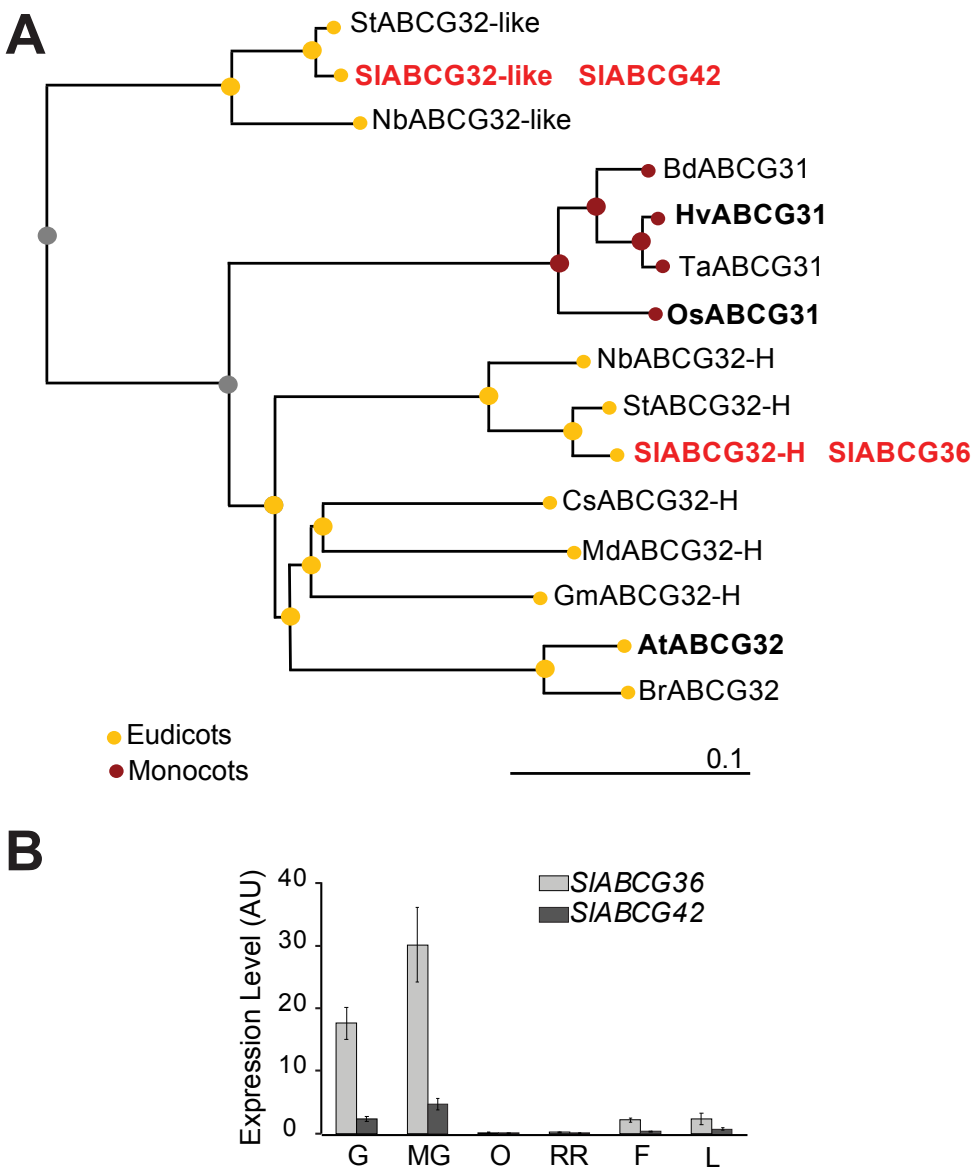

Figure S1. Two *AtABCG32* homologues exist in tomato, Related to Figure 1 and Figure 3

(A) Neighbor Joining-based phylogenetic tree representing proteins of monocots and eudicots having homology to AtABCG32 based on a BLAST search using blastp (protein-protein BLAST), using selected species. Results were filtered to match records with percentage identity between 65 and 100%. Tree was generated using the Blast tree view tool. Scale bar represents the number of differences between species (0.1 means 10% differences between two sequences). ABCG32-like: Nb, *Nicotiana benthamiana* BAR94054.1|; Sl, *Solanum lycopersicum* XP_010322739.1| (SlABCG42; gene product of Solyc06g065670); St, *Solanum tuberosum* |XP_006353655.1|. ABCG32-H: At, *Arabidopsis thaliana* |O81016.1| (Bessire et al, 2011), Br, *Brassica rapa* |XP_009140751.1|; Cs, *Cucumis sativus* |XP_004139333.1|; *Gm, Glycine max* |*XP_003524521.1*|; *Md Malus domestica* |*XP_028950701.1*|; Nb, |BAR94048.1|, Sl, |XP_010321067.1| (SlABCG36; gene product of Solyc05g018510) ; St, |XP_006338166.1|. ABCG31-H: Bd, *Brachypodium dista,* XP_003569645.1|; Hv, *Hordeum vulgare* |KAE8773549.1| (Chen et al. 2011); Os, *Oryza sativa,* |*Q8GU87.3*| (Chen et al, 2011, Garroum et al., 2016), Ta, *Triticum aestivum,* |*CDM81797.1*|. Red, *S. lycopersicum* proteins (Ofori et al., 2018); bold, experimentally characterized members.

(B) Expression of the *ABCG32* homologues, *SlABCG36* and *SlABCG42,* in different organs and fruit developmental stages in WT tomato plants. G, green fruits; MG, mature green fruits; O, orange fruits; RR, ripe red fruits; L, young leaves; F, fully open flowers. Histograms represent the mean expression level (in arbitrary units (AU) for 4 different samples for 3 different WT plants, and three technical replicates by sample. Error bars represent SD.

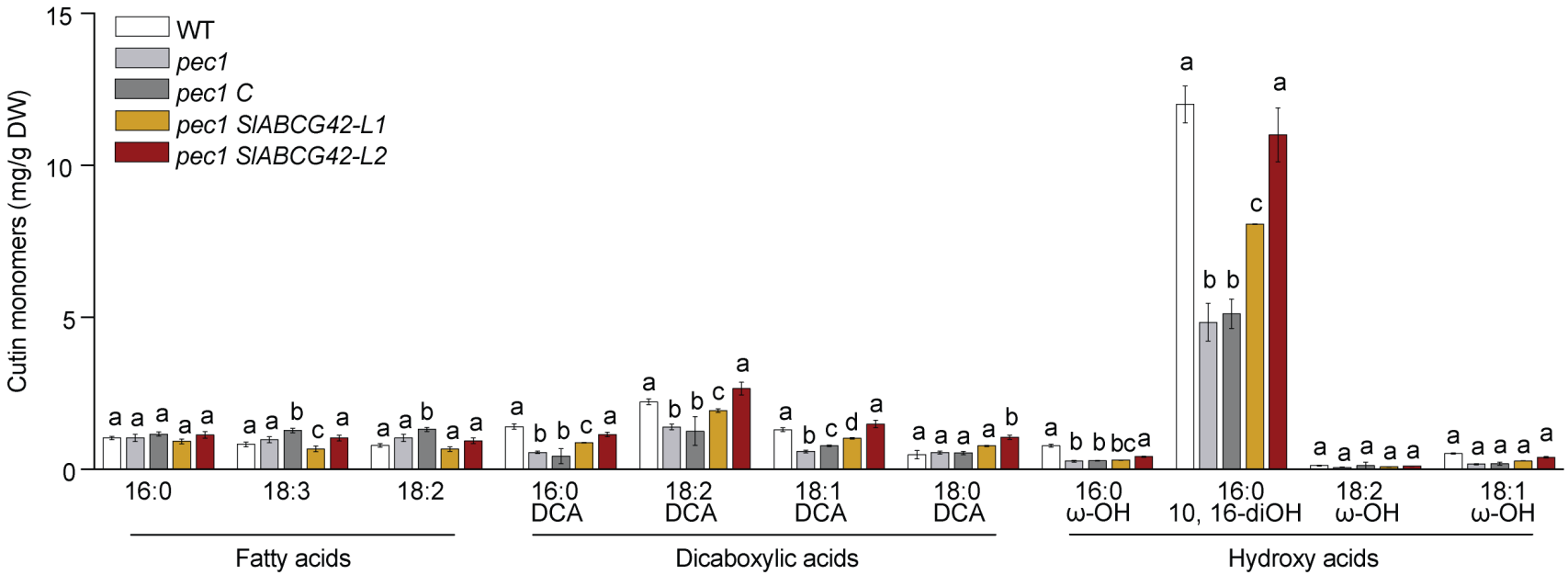

Figure S2. SlABCG42 complements *pec1/acbg32* mutant cutin composition, Related to Figure 1

Transgenic p*ec1* lines expressing *SlABCG42* (*pec1 SlABCG42-L1* and *L2*) under the native PEC1 promoter complement the monomer composition of flowers of the *pec1* mutant. *pec1* C, *pec1* mutant transformed with the empty vector. Statistically significant differences are indicated by different letters (Two-way ANOVA, Tukey HSD multiple comparison, $P<0.05$, n=5 replicates). The analysis was performed twice with similar results and a representative data set is shown.

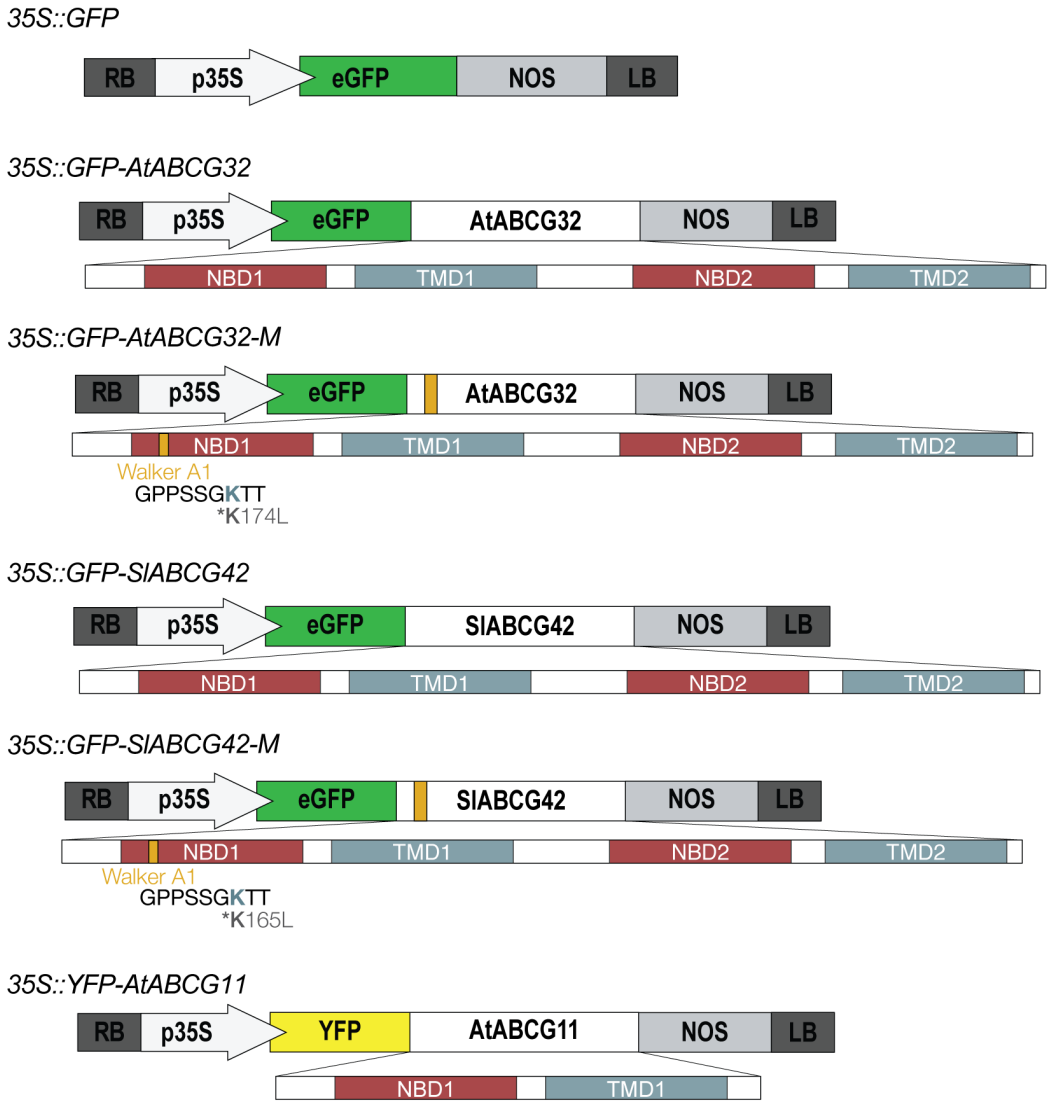

Figure S3. Schematic diagrams of the constructs used for the heterologous expression of ABCG transporters in *N. benthamiana*. Related to Figure 2.

Schematic diagrams of the constructs as well as the main domains of ABCGs and the location of the mutation (K174L) in the Walker A1 motif underneath each construct. NBD: Nucleotide-Binding domain; TMD: transmembrane domain.

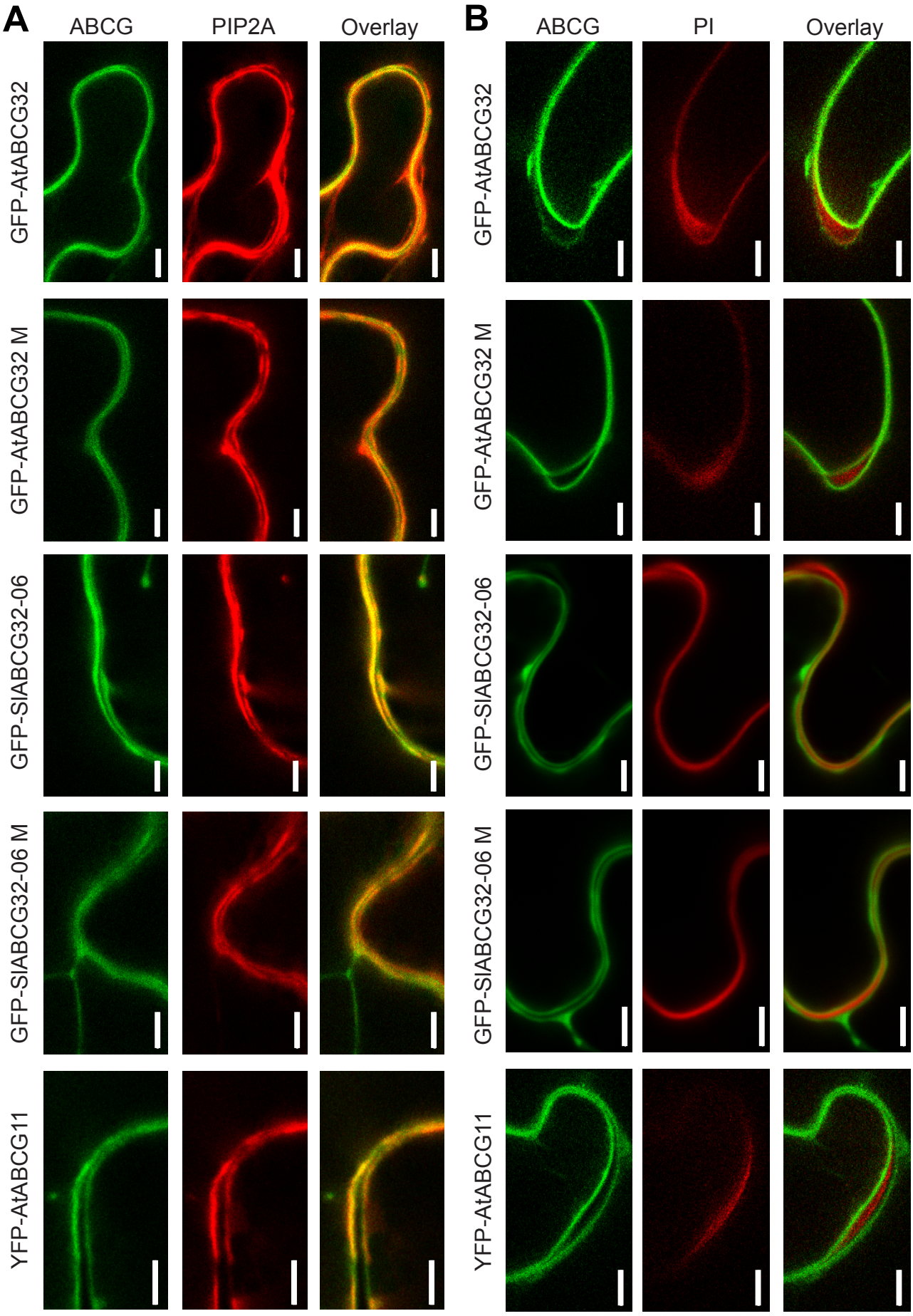

Figure S4. Localization of *Arabidopsis* ABCG transporters in *N. benthamiana,* Related to Figure 2

FP-tagged ABCG transporters were localized in *N. benthamiana* leaf epidermal cells using confocal-laser scanning microscopy. Co-localization of the FP-tagged ABCG-transporters with the mCherry-tagged plasma membrane marker PIP2A is presented in A. Localization of the FP-tagged ABCG-transporters adjacent to the cell wall visualized with propidium iodine is shown in B. Scale bars represent 5 µm.

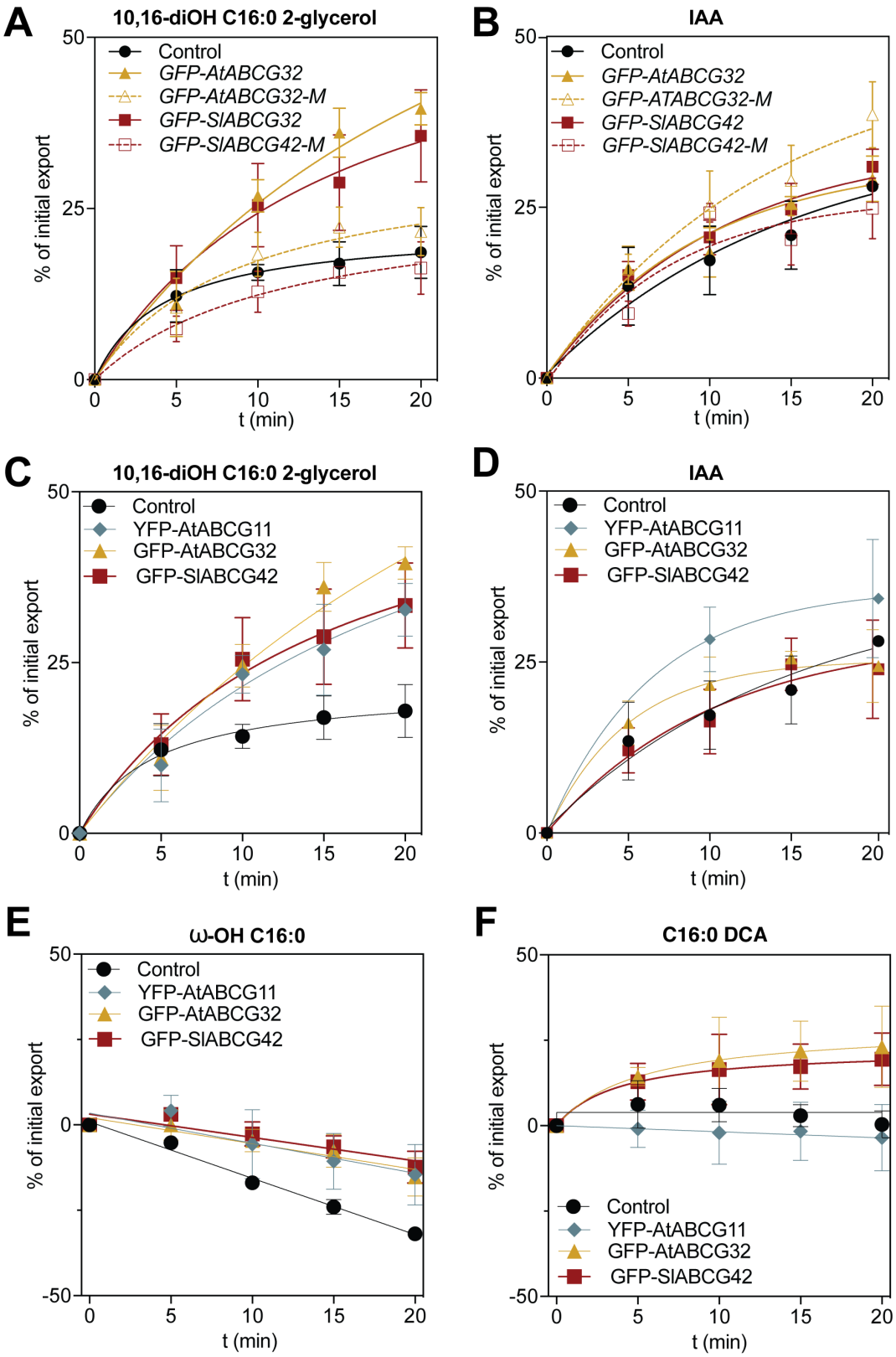

Figure S5. ABCG transporters required for cutin formation export fatty acid derivatives, Related to Figure 2

Heterologous expression of AtABCG32 and SlABCG42 as well as AtABCG11 in *N. benthamiana* protoplasts reveals export activity across the plasma membrane for 10,16 diOH C16:0 as well as ω-OH C16:0, while C16:0 DCA is only exported by AtABCG32 and SlABCG42. Percentage of initial export of different substrates across the plasma membrane of protoplasts expressing the empty vector (Control), GFP-AtABCG32, GFP-AtABCG32-M, GFP-SlABCG42, GFP-SlABCG42-M, and YFP-AtABCG11 at 0, 5, 10, 15 and 20 min. Three radiolabeled C16:0 substituted acids were used as substrates: **(A,C)** [^{3}H]-10,16-diOH 16:0-2-glycerol; **(E)** [^{14}C]-ω-OH C16:0; **(F)** [^{3}H]-C16:0 dicarboxylic acid (C16:0 DCA). **(B,D)** [^{14}C]-labeled indole acetic acid (IAA) was used as unrelated compound for comparison. Data represented as mean ± standard error of the mean.

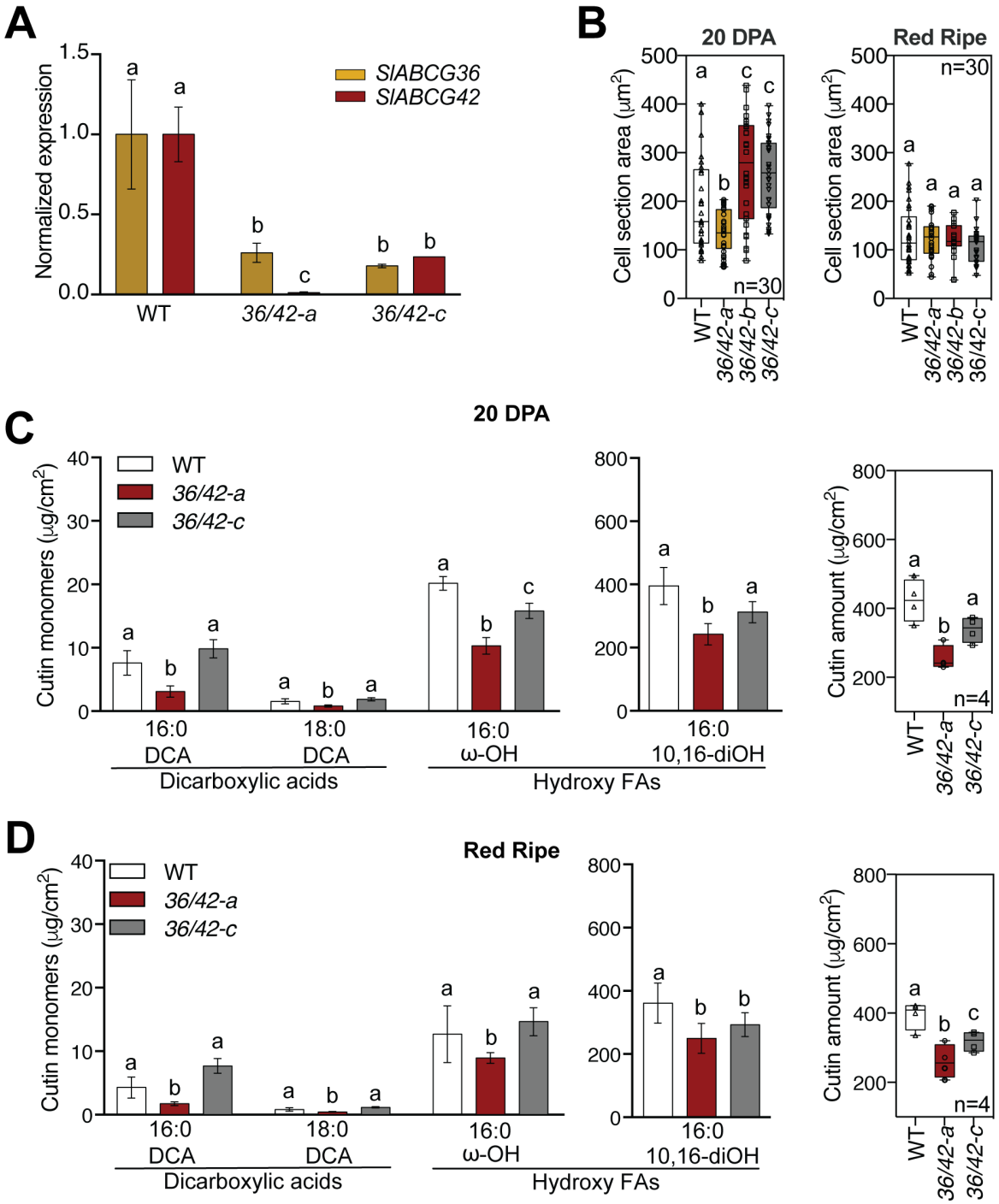

Figure S6. Reduced expression of *AtABCG32*-homologous genes as well as alterations in cell shape and reduction in cutin deposition in *slabcg36/42* plants, Related to Figure 3 and Figure 4

(A) Expression analysis of *SlABCG36* and *SlABCG42* in selected RNAi lines, i.e. *slabcg36/42-a* (*36/42-a*) and *slabcg36/42-c* (*36/42-c*) normalized to wild-type (WT) show significant differences between the RNAi lines in *SlABCG42* expression as well as of both genes to WT. Real time-qPCR was performed with two biological replicates for 2 plants belonging to the same T2 line and three technical replicates by sample. Error bars represent SD. Analyses were performed with 10 DPA fruits. Statistically significant differences are indicated by different letters (Two-way ANOVA, Tukey HSD multiple comparison, $P<0.05$, $n=4$ replicates). **(B)** Cell shape was evaluated by measuring the size of ultrathin sections of epidermal cell pictured in transmission electron microscopy. A high variability in cell section size is generated by the conical cells in WT and the intermediate downregulated *slabcg36/42* line, while the homogenous flat cells result in a small cell section size of low variability in the strongest downregulated line at 20 DPA. Statistically significant differences between cell section areas are indicated by different letters (One-way ANOVA, Tukey HSD multiple comparison, P<0.05, n=30 pictures) (**C**) and (**D**) The amount of cutin monomers (left) and the total cutin amount (right) of isolated cutins were quantified in 20 DPA-old **(C)** and in Red Ripe **(D)** fruits of the T2 plants characterized in (**A**). Statistically significant differences between amount of cutin monomers and total cutin amounts are indicated by different letters (Two-way ANOVA, Tukey HSD multiple comparison, $P<0.05$, $n=4$ replicates).

Gene name	Gene number
AtABCG32/PEC1	*At2g26910*
AtABCG11	*At1g17840*
SlABCG36	*Solyc05g018510*
SlABCG42	*Solyc06g065670*

Table S1. List of genes mentioned in this study, Related to Star Methods

Primer name	Primer sequence	Reference
pec1-2_LP	GTTGTGATGCATTGTTGTTCG	SALK primer design (SALK line SALK_025696.51.80.x)
pec1-2_RP	AAGCCTCGTCGTGGAGTATG	
LBAi	TGGTTCACGTAGTGGGCCATCG	
pAtABCG32+HindIII F	*ATAAGCTT*AGAAAGGTCTCGGGAGGAAAC	Bessire et al., 2011[S1]
pAtABCG32+KpnI R	*TTAGGTACC*AATCTCCGCGGCGGCGCAACAGAA	
SlABCG42 attB1 F	GGGGACAAGTTTGTACAAAAAAGCAGGCTACATGTCAACAAGAGGTGAAAATGG	Present work
SlABCG42 attB2 R	GGGGACCACTTTGTACAAGAAAGCTGGGTTTTTACACAAATAGCCAGTCGGAT	
SDM_AtABCG32 F	AAGTTCAGGGttGACAACATTACTCTTAG	Present work
SDM_AtABCG32 R	GGAGGACCTAGTAGTAGTG	
SDM_SlABCG42 F	TAGCTCTGGAttAACAACATTGCTTTTGGCACTTG	Present work
SDM_SlABCG42 R	GGCGGACCCAAAAGCAGC	
fragSlABCG36 F	AAAAAGCAGGCTACACATACCAGTGACCAAGT	Present work
fragSlABCG36 R	AGAAAGCTGGGTTAAGAGCTGAAAAAATTTGAAAAT	
fragSlABCG42 F	AAAAAGCAGGCTACAAACCTGTCCTACTGGAG	Present work
fragSlABCG42 R	AGAAAGCTGGGTTGGCTGCTCTTTCACGATA	
TIP41 qPCR F	AGATGAACTGGCAGATAATGG	Expósito-Rodríguez et al., 2008[S2]
TIP41 qPCR R	CATCAACCCTAAGCCAGAAA	
SlABCG36 qPCR F	GACTACTGCAATCACACCCA	Present work
SlABCG36 qPCR R	CCATCGGATAGTTTCACCAG	
SlABCG42 qPCR F	CGCTCTTCGGTATGATGACA	Present work
SlABCG42 qPCR R	AACACCATCAGCGAGCGTAA	

Table S2. Primers used in this study, Related to Star Methods

Special information about the primer sequences are indicated as follows: italic, restriction enzymes sites; underlined, sequence corresponds to AttB sites for recombination cloning; lower case, exchanged nucleotides.

Supplemental References

S1. Bessire, M., Borel, S., Fabre, G., Carraca, L., Efremova, N., Yephremov, A., Cao, Y., Jetter, R., Jacquat, A.C., Metraux, J.P., et al. (2011). A member of the PLEIOTROPIC DRUG RESISTANCE family of ATP binding cassette transporters is required for the formation of a functional cuticle in Arabidopsis. Plant Cell *23*, 1958-1970.

S2. Exposito-Rodriguez, M., Borges, A.A., Borges-Perez, A., and Perez, J.A. (2008). Selection of internal control genes for quantitative real-time RT-PCR studies during tomato development process. BMC Plant Biology *8*, 131.